

Energy & Environmental Science

Accepted Manuscript



This is an *Accepted Manuscript*, which has been through the Royal Society of Chemistry peer review process and has been accepted for publication.

Accepted Manuscripts are published online shortly after acceptance, before technical editing, formatting and proof reading. Using this free service, authors can make their results available to the community, in citable form, before we publish the edited article. We will replace this *Accepted Manuscript* with the edited and formatted *Advance Article* as soon as it is available.

You can find more information about *Accepted Manuscripts* in the [Information for Authors](#).

Please note that technical editing may introduce minor changes to the text and/or graphics, which may alter content. The journal's standard [Terms & Conditions](#) and the [Ethical guidelines](#) still apply. In no event shall the Royal Society of Chemistry be held responsible for any errors or omissions in this *Accepted Manuscript* or any consequences arising from the use of any information it contains.

Recent progress in solar cells based on one-dimensional nanomaterials

Hao Sun, Jue Deng, Longbin Qiu, Xin Fang, Huisheng Peng*

State Key Laboratory of Molecular Engineering of Polymers, Department of Macromolecular Science, and Laboratory of Advanced Materials, Fudan University, Shanghai 200438, China; E-mail: penghs@fudan.edu.cn.

Abstract: To develop solar cells with high power conversion efficiencies is critical but remains challenging for the sustainable development of human society. It is well recognized that rapid charge separation, transport and collection are beneficial to highly efficient solar cells, which requires optimization at microscopic structures and morphologies. One-dimensional nanomaterials favor charge transport and collection derived from large specific surface areas and one-dimensional configuration, which have been widely used to fabricate solar cells. In this review, the recent progress in high-performance solar cells based on one-dimensional nanomaterials is comprehensively described with an emphasis on the mostly explored metal, metal oxide, carbon and conductive polymer. The impact of one-dimensional structure on device performance is highlighted to elucidate the advantages of such nanomaterials. The future development of one-dimensional nanomaterials towards next-generation solar cells is finally summarized.

1. Introduction

Energy crisis has become one of the most serious problems that threaten the future development of human society. With the exhaustion of non-renewable fossil fuels, more and more attentions are paid to develop renewable and environmentally friend energy sources, e.g., wind, geothermal, tidal and solar energy. Solar energy is well recognized as one of the most promising choices to meet the enormous energy demand in the future. To this end, developing efficient solar cells with high power conversion efficiency (PCE) is highly demanded. Efficient charge separation, transport and collection processes are beneficial for the improvement of PCE, which requires the optimization at both material and configuration.¹⁻³ On this account, one-dimensional nanomaterials share various advantages based on their unique one-dimensional configuration, which enables rapid charge transport along the axial direction. Furthermore, the nanoscale effect provides large specific surface area and other fascinating properties, making them suitable for efficient solar cells. To date, various advancements have been achieved using one-dimensional nanomaterials for

photovoltaic applications. Herein, the recent advancements of the third generation solar cells based on one-dimensional nanomaterials, including dye-sensitized solar cells, polymer solar cells and perovskite solar cells, have been systematically reviewed. Three representative one-dimensional nanomaterials, i.e., metal and metal oxide, carbon and conductive polymer, are discussed. The impact of one-dimensional structure on the device performance is highlighted to elucidate the advantages of the one-dimensional configuration in efficient charge separation, collection and transport. The outlook for one-dimensional nanomaterial-based solar cells is provided at the end of the review.

1.1. Structure and working mechanism of three kinds of solar cells

For the convenience of discussion, the principles of dye-sensitized solar cells, polymer solar cells and perovskite solar cells are first summarized here. The structure and working mechanism of dye-sensitized solar cell (DSC) have been already described in many reviews.⁴⁻⁶ A typical configuration of DSC exhibits a sandwich structure developed by Grätzel and co-workers. Two electrodes—photoanode and counter electrode—are placed in parallel and separated by electrolyte. Transparent conducting glass with fluorine-doped tin dioxide (FTO) or indium-doped tin oxide (ITO) on one side usually serves as the substrate for the deposition of a thin film of mesoporous semiconductor oxide. The counter electrode is deposited with a catalytic layer like platinum or carbon materials. After the photoanode is absorbed with dye molecules, the electrolyte is injected and two electrodes are sealed. When the cell is under illumination, the dye molecules capture photons and then inject electrons into the conduction band of the semiconductor. Electrons migrate through the semiconductor layer and travel throughout the external circuit. The route for electron transport inside the cell is closed by the redox cycle in the electrolyte. The triiodide ions, the hole conductors, obtain electrons and are reduced to iodide ions at the counter electrode. The iodide ions release electrons to regenerate the oxidized dye molecules afterwards. In these processes, the charge injection and transport are always accompanied by the charge recombination, which decays the output performance of the DSC.

A typical polymer solar cell contains three parts, i.e., anode (modified with hole transport material like PEDOT:PSS and MoO_3), cathode (modified with electron transport material like TiO_2) and active layer (containing electron donor and acceptor) (Fig. 1b). The preparation of each layer can be performed through a solution process in sequence. The hole transport materials are beneficial for hole selecting transport and electron transport blocking, while the electron transport materials function as electron selecting transport and hole blocking to improve charge collection. To

enhance the light harvest and carrier separation, the active layer is constructed into a separated interpenetrating network at the nanoscale due to a relatively short carrier diffusion length of the active materials. During light absorption and excitation, the excitons, which are tightly bonded electron-hole pairs in the active layer, are transferred to the interface of donor and acceptor, followed by separating into electrons and holes and collected by the electrodes. The crystalline of active layer and size of nanoscale phase are considered to be vital for carrier generation, transport and separation, which conjointly determine the efficiency of the devices.⁷⁻¹⁰

A perovskite solar cell has been produced with perovskite materials as light harvester.¹¹⁻¹² A relatively thin layer of mesoporous TiO₂ film is deposited on the top of a compact layer (as blocking layer) on a transparent conductive oxide (TCO) glass substrate. The blocking layer prevents direct electrical contact between TCO and hole transporting material, which reduces charge recombination at the interface. An absorber layer is formed by adsorbing a monolayer of sensitizer on mesoporous TiO₂ layer, and the solution of hole transporting material is infiltrated into the pores, which is critical for the transfer of the holes to the hole transporting material, followed by electron injection into the TiO₂ film. As a result, a thin photoanode layer is prerequisite to facilitate pore filling and generate a suitable diffusion length to restrain charge recombination. Finally, a thin film of a metal (Au or Ag) counter electrode is deposited to collect the generated charges (Fig. 1c).

1.2. Advantages and contributions of one-dimensional nanomaterials in solar cells

The one-dimensional configuration and nanomaterial characteristics have made one-dimensional nanomaterials very promising as the building blocks to enhance the performances of solar cells. Herein, a general perspective to the advantages and contributions of one-dimensional nanomaterials in solar cells is provided.

Balance between transparency and conductivity. The transparent conductive electrodes are widely used in the fabrication of various solar cells, and the transparency and electrical conductivity are two important factors determining the device performance. A high transparency represents less loss of the incident light, and a low resistance means lower internal resistance of the solar cell. The dilemma between the transparency and resistance has always been a problem. Thinner transparent conductive layer demonstrates higher transparent, but the sheet resistance will be increased. Thicker transparent conductive layer shows lower sheet resistance, while the high transparency has to be sacrificed. The one-dimensional nanomaterials, including Ag and Cu nanowire networks, not only provide fast charge transport

highway, but also offer enough interspace among nanowires for the penetration of incident light, which can strike an excellent balance between the two factors. Up to date, a high transmittance of over 90% and low electrical resistance of $\sim 10 \Omega \square^{-1}$ have been achieved based on Ag nanowires, which are comparable to ITO under the same condition.^{13,14} Thus, one-dimensional nanomaterials have been widely investigated as the transparent conductive electrode materials to enhance the performances of solar cells.

High specific surface area. The interface between two phases has always been considered to be crucial for various systems, not limited to photovoltaic conversion. Larger specific areas enable sufficient charge generation, separation and collection, which lead to high device performances.¹⁵ Comparing with conventional bulk materials, materials in nanoscale demonstrated much larger specific surface areas with higher interacting efficiencies, thus are favorable for performance enhancement. Although the specific surface areas of one-dimensional nanomaterials are generally lower than their zero-dimensional counterparts, some strategies can be adopted to overcome this problem. One representative example is the roughened hierarchical structure of TiO₂/ZnO nanowires which takes the advantages of both dye adsorption and fast electron transportation together to enhance the device performances.

Direct charge transport path. For nanoparticles, the electrical resistances are generally high due to the existence of many grain boundaries which restrain the rapid charge transport.^{16,17} One-dimensional configuration provides direct charge transport path and decreases the electrical resistances compared with nanoparticles. TiO₂ nanorod, nanowire and nanotube have been widely investigated as promising photoanode materials in the replacement of conventional TiO₂ nanoparticles towards efficient DSCs.

Orientated structure. The assemble method of nanomaterials is considered to be very important to extend their physical properties from nanoscale to macroscopic scale. Orientated structure has been proofed to efficiently improve the mechanical and electrical properties of nanomaterials on the orientated direction, which is favorable for the improvement of device performances.¹⁸ The anisotropic configuration is a necessary factor for the formation of orientated structure. To this end, one-dimensional nanomaterials have demonstrated large potential to be assembled into highly orientated structure with much improved properties and device performances. Up to date, orientated one-dimensional metal oxide, carbon and polymer nanomaterials have all been prepared and served as sufficient components to build solar cells with high performances, which will be discussed in the corresponding section.

2. One-dimensional metal and metal oxide

2.1. Metal

Transparent, flexible and low-cost conducting electrodes are highly desired with the burgeoning of flexible and large-scale photovoltaic devices. Traditional transparent conductive oxides (TCO) can hardly satisfy various requirements for flexible applications due to the fragile property as well as high cost. Alternately, one-dimensional metal nanomaterials like silver and copper nanowires exhibit great potentials as transparent and flexible electrodes because of their intrinsic high conductivity and flexibility. In this section, one-dimensional metal nanomaterials aiming at enhancing the PCE are discussed.

2.1.1. Silver nanowire

With the high conductivity and suitable work function, silver materials have been widely used in photovoltaic devices. However, Ag nanoparticle is an inferior choice due to the dilemma to reach both high optical transmittance and electrical conductivity in the resulting electrode. Fortunately, when the zero-dimensional nanoparticles are replaced by one-dimensional nanowires, the transmittance has been largely enhanced at the same high conductivity, e.g., a transmittance of over 90% and low electrical resistance of $\sim 10 \Omega \square^{-1}$, which are comparable to ITO under the same condition^{13,14} (Fig. 2a). The improvement is ascribed to the one-dimensional configuration that favors the formation of a network structure, and the space in the nanowire network increases the optical transparency (Fig. 2b). The transparent network electrodes based on Ag nanowires have been explored for dye-sensitized and polymer solar cells.

A solution process such as spraying deposition of Ag nanowires is typically used to fabricate flexible electronics aiming at a large-scale production (Fig. 2c and d).^{13,19-21} The conventional solid-state dye-sensitized solar cells require a sintering treatment at 450 °C, which is too high for most plastic substrates to achieve flexible solar cells. Therefore, a Ag nanowire/poly (3, 4-ethylenedioxythiophene) polystyrene sulfonate (PEDOT:PSS) electrode had been made by spraying process to fabricate solid-state dye-sensitized solar cells at low temperatures.^{22,23} Ag nanowires were able to achieve a low sheet resistance without annealing, while PEDOT:PSS was used to reduce the contact resistance and enhanced the lateral charge transport. Ag nanowires can be also directly coated onto polymer substrates to fabricate flexible devices, achieving a PCE of 5.02%, comparable to the glass substrate-based counterpart.¹³

Besides serving as transparent electrodes, Ag nanowires can be also used in building efficient electron acceptor layer of polymer solar cells. Kim et al. embedded Ag nanowires in P3HT:PCBM films, which served as an electron acceptor to enhance the performance of the hybrid solar cells.²⁴ Moreover, the excellent plasma properties of Ag in the visible spectra engender surface plasma resonance which efficiently increases light absorption. Kang et al. added periodic Ag nanowire gratings in polymer solar cells.²⁵ One Ag layer was continuous as a top electrode, and the other Ag layer on the glass was made into a periodic structure to couple the incident plane wave to surface plasma waves. The photovoltaic performance had been enhanced by 35% under non-polarized light illumination compared with the ITO-based device.

2.1.2. Copper nanowire

The transparent conducting electrode based on Cu nanowires is another superior substitution of ITO (Fig. 3a and b).²⁶⁻²⁸ The abundant resource and low cost of Cu nanowire have motivated the investigation of their applications on both dye-sensitized and polymer solar cells. Exciting results including sheet resistance of $100 \Omega \square^{-1}$ and transmittance of 95% have been achieved.²⁹ However, the oxidation of copper undermines the stability and the indispensable annealing process in H_2 hinder their applications. To this end, some efforts have been made to improve the stability and simplify fabrication process of Cu nanowires. For instance, Cu nanowires were incorporated into conductive PEDOT:PSS and baked stepwise to prevent the degradation.²⁷ The PCE reached 3.1% compared with 4.0% based on conventional ITO substrate. Furthermore, to prevent oxidation, Ni was deposited on Cu nanowires and acetic acid treatment replaced the hydrogen annealing. The PCE of 4.9% was comparable to that on the basis of Ag nanowires (Fig. 3c).³⁰

2.2. Metal oxide

Metal oxide nanomaterials have been widely used as semiconductors in solar cells. One-dimensional metal oxide nanostructures including nanorods, nanowires, nanotubes and nanobelts exhibit unique properties and attracted intensive investigations. In this section, one-dimensional titanium oxide and zinc oxide are described and highlighted for applications in solar cells as two demonstrations.

2.2.1. Titanium dioxide

TiO₂ nanofiber

It is well recognized that the morphology of the semiconducting thin film is critical for the device performance. TiO_2 nanoparticles are widely used in dye-sensitized, polymer and perovskite solar cells. However, to certain extent, it exhibits some shortcomings. One of the significant disadvantages is the numerous grain boundaries, surface defects and trap states hindering electrons transport among particles, leading to severe recombination. One-dimensional TiO_2 nanomaterials have successfully solved this problem by improving the charge transport with straight pathways and enhancing light harvest by light scattering.

Electrospinning represents a simple and economical method to synthesize nanofibers, which is also compatible to doping, modification, morphology control and scale-up production. After tackling the poor adhesion of nanofibers on substrates by calcination, recent studies aimed at preparing delicate nanofibers to enhance the PCE.³¹ Yang et al. incorporated carbon nanotubes into TiO_2 through an electrospinning process (Fig. 4a).³² The resulting dye-sensitized solar cell with this hybrid film as a photoanode showed a PCE up to 10.24%, with high short-circuit current density and fill factor of 18.53 mA cm^{-2} and 0.74, respectively. The remarkable PCE was attributed to the enhancement of charge transport by the introduction of carbon nanotubes.

The enhanced charge transport of TiO_2 nanofibers was at the cost of reducing specific surface area. To this end, the synthesis of porous TiO_2 nanofibers can well overcome this shortcoming. Lin et al. synthesized wormhole-like mesoporous anatase TiO_2 nanofibers using room-temperature ionic liquids as mesopore-forming templates. The obtained porous TiO_2 nanofibers combined the merits of mesoporous materials and one-dimensional structure which were beneficial to dye absorption and charge transport, resulting in PCE of 5.6%.³³ Another hollow fiber even utilized the inter surface on the basis of natural cellulose fibers as templates. A longer photoinjected electron lifetime with the high surface area boosted the PCE to 7.2% in the resulting dye-sensitized solar cell.³⁴ In addition, SiO_2 nanoparticles with various sizes also represent effective templates. After etching the electrospun $\text{SiO}_2/\text{TiO}_2$ hybrid fiber, the surface area of TiO_2 nanofibers with multi-sized pores showed a nine-fold increase compared with bare TiO_2 nanofibers, ensuring a sufficient dye adsorption and electrolyte contact. As a result, the resulting devices exhibited PCEs up to 8.5% (Fig. 4b).³⁵

It is well recognized that reasonable control on device architectures significantly promotes the photovoltaic performance.³⁶ As light scattering materials, thicker TiO_2 nanofibers exhibit better light scattering ability, while longer and thinner nanofibers absorbed more dye molecules due to a larger specific area.^{37,38} Yang et al. designed an innovative bilayer TiO_2 nanofiber-based DSC, which combined both small and large

diameters of TiO₂ nanofibers (Fig. 4c).³⁸ The small nanofibers with a diameter of 60 nm were used for dye absorption while the large nanofibers with a diameter of 100 nm worked as light scattering materials. This architecture was able to trap more light and promote the device performance.

Besides the applications in DSCs, TiO₂ nanofibers can be also used to build high-performance perovskite solar cells. The porosity of the electrospun nanofiber network after TiCl₄ treatment provided large surface area for compact contact with CH₃NH₃PbI₃ and favored a direct electron collection.³⁹ Combining the high absorption coefficient of perovskite material with high charge transport from porous TiO₂ nanofibers, the all-solid-state perovskite solar cell showed a high PCE of 9.8%.

Oriented TiO₂ nanowire

Many methods including sol-gel⁴⁰, hydrothermal⁴¹ and thermal evaporation method⁴² have been recently developed to synthesize oriented TiO₂ nanowires. Compared with a randomly dispersed TiO₂ nanofiber network, the oriented organization of TiO₂ nanowires can enhance the electron transport along the axial direction. As a result, when TiO₂ nanowires are used for the solar cells, high PCEs can be achieved.

The structure of TiO₂ nanowires also plays a critical role on the photoelectric performance of the resulting photovoltaic device. For instance, the formation of single crystal in TiO₂ is recognized to reduce the probability of trapping state, increase electron transport and suppress charge recombination for high PCEs.^{43,44} For the rutile TiO₂ nanowire array with the (001) face along the oriented direction, the diffusion length of free carriers was discovered to be 5 times shorter than that in TiO₂ nanoparticles (Fig. 5a-c).^{36,45} However, the smooth surface of single crystal TiO₂ nanowires is unfavorable for the dye absorption, which may lower the PCE of the dye-sensitized solar cell. A general and effective solution has been provided by modifying the nanowires for higher specific surface areas to improve the dye absorption and electrolyte diffusion. A synergistic interaction between titanium trichloride and octanoic acid was found to increase the surface area,⁴⁶ and TiO₂ nanowire arrays could be modified with a thin Nb₂O₅ layer to reduce surface recombination and shift conduction band edge.⁴⁷ The TiO₂ nanowires can be also etched into bunched secondary nanowires with much smaller diameters, and the resulting dye-sensitized solar cell displayed a PCE of 7.91% (Fig. 5d and e).⁴⁸ Of course, denser TiO₂ nanowire arrays synthesized with the assistance of acetic acid obviously increased the specific surface area.⁴⁹

Oriented TiO₂ nanotube

Oriented TiO₂ nanotubes have been also widely studied as attractive one-dimensional materials for the use in photovoltaic devices due to the similar reasons in oriented nanowires: (1) the fabrication is reliable with tunable structures; (2) large surface area enhances the loading capability of photoactive materials; (3) vertically oriented TiO₂ nanotubes facilitate the charge separation and transport. Anodic oxidation represents the most widely investigated method to synthesize these TiO₂ nanotubes. The length, diameter, doping and modification of TiO₂ nanotubes can be tuned by varying the experimental parameters such as applied voltage, grown time and electrolyte.

Vertically grown TiO₂ nanotube arrays on Ti foils are typically used as photoanodes in dye-sensitized solar cells. The length, orientation degree, surface morphology and crystallinity are critical to their photoelectric performances (Fig. 6a),^{50,51} and a lot of efforts have been made to optimize them. For instance, a surface engineering can be made by TiCl₄ treatment⁵¹, oxygen plasma exposure⁵² and additional hydrothermal treatment.^{53,54} After these treatments, the TiO₂ nanotubes were roughened with small rutile nanocrystals on the wall and at the top. The surface modification offered a high PCE of 7.24% (Fig. 6b).

As the sunlight cannot penetrate through the Ti substrate, the incident light must enter from the counter electrode side in a dye-sensitized solar cell. However, both electrolyte and counter electrode impede the light absorption. Therefore, oriented TiO₂ nanotubes had been transferred onto transparent substrates by ultrasonic or H₂O₂ treatment.⁵⁵⁻⁵⁷ However, the closed end of TiO₂ nanotubes produced relatively short electron lifetime. Fortunately, a facile flaking process was applied to open their ends to increase the PEC to 9.1%, compared with 5.3% for the case of closed ends.^{57,58}

TiO₂ nanotube arrays can also serve as electron collection materials in perovskite solar cells. For instance, free-standing TiO₂ nanotube arrays were synthesized through a two-step anodization process, and the device performance strongly depended on the length of TiO₂ nanotubes as expected. Shorter nanotubes favored the charge transport but reduced the adsorption of active materials, while longer nanotubes increased the adsorption but lengthened the transport pathway. After a comparing study, the maximal PCE of 6.52% occurred at the length of 2.3 μm.

Hierarchical one-dimensional TiO₂ nanostructure

Hierarchical one-dimensional nanostructures typically display tree-like shapes with secondary even tertiary branches on the one-dimensional backbone such as nanowires and nanotubes. The backbones provide efficient pathways for electron transport while

the branches offer high specific surface areas for dye loading. The hierarchical architectures also exhibit multiple interactions with the incident light for higher photovoltaic conversion efficiencies.

Hierarchical one-dimensional TiO₂ nanostructures were typically realized by hydrothermal method,⁵⁹⁻⁶⁴ and the PCEs of the resulting dye-sensitized solar cells were ranged from 4 to 8%, higher than those based on TiO₂ nanowires (Fig. 6c).^{59,60,62} According to this strategy, hyperbranched TiO₂ nanostructures with branched short nanorods from secondary stems were designed to further enhance the collecting and transporting efficiency of photo-injected electrons (Fig. 6d). These secondary and tertiary branches also enhanced light scattering verified by the higher monochromatic incident photon-to-electron conversion efficiency (IPCE) (Fig. 6e). As a result, a higher PCE of 8.11% was achieved (Fig. 6f).⁶⁴ Moreover, an oriented nanowire-nanosheet-nanorod hyperbranched array and ultra-long multi-layered anatase TiO₂ nanowires promoted the PCE to 9.09% and 9.40%, respectively.^{65,66}

Hybridizing one-dimensional nanostructure materials with high surface areas represents another strategy for higher PCEs. Freestanding TiO₂ nanotube arrays were modified onto TiO₂ nanoparticles to extend the photoelectric lifetime by 237.5%, resulting in the PCE of 8.80%.⁶⁷ Dendritic microspheres had been also used to replace nanoparticles to enhance light scattering, but to certain degree, sacrificed the specific surface area.⁶⁸ When both branched hollow spheres and microspheres were deposited at the top of hydrobranched nanowire arrays, the PCE reached 11.01%.⁶⁶

2.2.2. Zinc oxide

One-dimensional ZnO nanomaterials have received extensive attentions due to both higher electron mobility and longer electron lifetime compared with TiO₂. In particular, ZnO can be directly used to absorb dye molecules without annealing, which is generally required for the transformation of crystal form in TiO₂, aiming at high PCEs.

Oriented ZnO nanowire

Many approaches are available to synthesize ZnO nanowires,⁶⁹ and the hydrothermal method has been mostly explored due to the availability for various substrates. For instance, oriented ZnO nanowire arrays were grown on stainless steel wires or meshes to fabricate flexible and transparent dye-sensitized solar cells, so they can stably work under illumination from both sides.^{70,71} However, the mismatch of energy levels between ZnO and stainless steel hindered the electron diffusion, resulting in a poor

photovoltaic performance. Three-dimensional dye-sensitized solar cells with ZnO nanowire arrays grown on various substrates including Kevlar fiber, optical fiber and quartz slide were also produced (Fig. 7a and b).⁷²⁻⁷⁴ This three-dimensional fiber-shaped configuration enabled internal reflection at the interfaces, creating more opportunities for energy conversion. The PCE had been enhanced by six times compared with the illumination from the outside. The three-dimensional dye-sensitized solar cells using the planar quartz slide grown with ZnO nanowire arrays on both sides also guided the internal reflection and increased charge collection. A PCE of 2.4% was produced but needed to be further increased.

To this end, four layers of ZnO nanowire arrays were synthesized through a multi-batch process to increase the PCE to 7%. The significant improvement was attributed to a higher specific surface area in the four-layered photoanode compared with a single-layered photoanode⁷⁵ (Fig. 7c). The coat of a thin layer of semiconductors or insulators such as TiO₂^{76,77}, MgO⁷⁸, ZnS⁷⁹, ZnTe⁷⁹ and ZrO₂⁸⁰ was demonstrated to hinder carrier recombination and increase dye absorption, producing a PCE up to 7.3%. It had been also verified that the doping of Group III metals including In, Ga and Sn onto ZnO nanowires enhanced the device performance.⁸¹ Here N and P-doped ZnO exhibited the characteristic of p-type semiconductors.^{82,83}

The high electron mobility in oriented ZnO nanowires provides them promising applications in polymer solar cells that generally exhibit short exciton diffusion length. The oriented ZnO nanowires offer high interfaces for charge separation and provide continuous percolation pathways. In a bulk heterojunction solar cell, oriented ZnO nanowires are filled with poly (3-hexylthiophene) (P3HT) as the photoactive layer through a slow drying process for the maximal ZnO/P3HT interface, while electron acceptor such as [6,6]-phenyl-C₆₁-butyric acid methyl ester (PCBM) or indene-C₆₀ bisadduct (ICBA) was introduced to form the bulk heterojunction blend.⁸⁴ Here ZnO served as electron conductor to promote electron transport (Fig. 7d).

Oriented ZnO nanowires have also been used in perovskite solar cells with high performances. For example, CH₃NH₃I and PbI₂ were coated on the FTO glass grown with oriented ZnO nanowires, and the perovskite-infiltrated ZnO nanorods showed a remarkable PCE of 11.13%. The high performance was ascribed to an efficient electron collection of oriented ZnO nanowires.⁸⁵

Hierarchical one-dimensional ZnO nanostructure

Hierarchical one-dimensional ZnO nanostructures show the same construction to TiO₂. The re-nucleating process is mainly used to realize the formation of such hierarchical

nanostructures. First, the primary ZnO nanowire arrays were grown on the substrate, and then various seeds or re-nucleating sites had been introduced to the primary structure to grow the branches.

Several methods have been developed to synthesize branched ZnO nanorods on the stem, but the morphologies are often varied, leading to different PCEs. For instance, branched ZnO nanowires were synthesized on FTO substrates via a solvothermal method.⁸⁶ The short-circuit current density was increased due to the higher internal specific surface area, and the PCE reached 1.5%, almost twice of the ZnO nanowire array. Tree-like ZnO nanowires had been also synthesized via hydrothermal method, and the PEC was five times of upstanding ZnO nanowires (Fig. 8a and b).⁸⁷ Two-step electrodeposition process could be used to synthesize branched ZnO nanowire arrays with nanoporous layers for a PCE of 4.08%.^{88,89} Multi-layered ZnO nanowire arrays were made into a “caterpillar-like” structure that produced a high PCE of 5.20% (Fig. 8c and d).⁹⁰

3. One-dimensional carbon nanomaterial

3.1. Carbon nanotube

Since Iijima elucidated the structure of carbon nanotubes (CNTs) in 1991, both the scientific and industrial communities have witnessed the perspective development of CNTs in the past two decades.⁹¹ Considered as seamless cylinders wrapped from graphene sheets, CNTs have sp^2 hybridized carbon atoms covalently bonded with each other. According to the number of graphene layers, CNTs can be categorized into single-walled and multi-walled. CNTs are well known for the intrinsic physical and chemical advantages, which were well demonstrated in many related reviews.⁹²⁻⁹⁵ CNTs show excellent mechanical properties with high Young's modulus and tensile strength on the level of 270-950 GPa and 11-63 GPa, respectively.⁹⁶ CNTs also display excellent electronic properties. By varying its chiral structure, a single-walled CNT can be controlled to be metallic or semiconducting,⁹⁷ and the metallic CNT shows superior capacity to carry an electric current density of 4×10^9 A cm^{-2} , which is 1000 times higher than metal materials.⁹⁸ For multi-walled CNTs, electrical conductivity up to 10^5 S cm^{-1} has been achieved, as well as high current densities on the level of 10^6 A cm^{-2} .⁹⁹ With a high surface area and numerous exposed carbon atoms at ends, CNTs exhibit superior catalytic activities, which is comparable to platinum in iodine/triiodide redox couple, an important reaction for the dye-sensitized solar cell.¹⁰⁰ The excellent mechanical, electronic and catalytic properties enable CNTs to show unique advantages in fabricating efficient solar cells.

3.1.1. Transparent carbon nanotube film

Different from the conventional solar cells based on p-n junctions and light absorption by semiconductor materials, the third generation solar cells require at least one transparent electrode for incident light. Since the decrease in resistance will sacrifice the transmittance, a compromise has to be made to balance the sheet resistance and transmittance of the transparent electrode. To date, FTO and ITO are still the most widely used transparent materials with a low sheet resistance around $10 \Omega \square^{-1}$ and a high transmittance over 90%.¹⁰¹ The high electrical conductivity and one-dimensional nanostructure have enabled carbon nanotubes to serve as a novel transparent electrode material.

Bare CNT films, like buckypaper and aligned CNT sheet, have been widely investigated to replace conventional transparent electrodes. Buckypaper is prepared by filtrating the CNT dispersion to form a flexible and porous mat. Containing both semiconducting and metallic CNTs, the electrical conductivity is ranged at the level of 10^3 S cm^{-1} .¹⁰² With many efforts to improve the properties, the sheet resistance ($\sim 500 \Omega \square^{-1}$) and transmittance (85%) of buckypaper have already met the physical requirements of transparent electrodes.¹⁰³ However, the area of the buckypaper is largely limited by the filtration equipment, especially for the continuous fabrication of large-sized solar cells.

To this end, various methods including drop-casting, transfer-printing, spray-coating and brush-painting are developed to satisfy practical applications.¹⁰⁴⁻¹⁰⁸ For instance, transparent single-walled CNT electrodes had been deposited on glasses by spray-coating,¹⁰⁶ and the resulting films were mechanically robust with high conductivities of $7694 \pm 800 \text{ S cm}^{-1}$. A low sheet resistance of $57 \pm 3 \Omega \square^{-1}$ and reasonable transmittance of 65% had been achieved. The CNT-based electrodes were further used to fabricate polymer solar cells by coating PEDOT:PSS, a blend of P3HT and PCBM, and LiF/Al on the CNT film. The resulting solar cell delivered a PCE of 2.2%, which was comparable with 2.3% using ITO-coated electrode. In addition, the CNT films could be made into freestanding and flexible, which is unavailable for ITO while highly desired in modern electronics such as portable and wearable electronic devices. Therefore, the CNT film may represent a promising candidate to replace ITO in the future.

3.1.2. Electrocatalytic carbon nanotube film

Conventional counter electrode of DSC, generally composed of a 2-3 nm layer of platinum deposited on a transparent conducting oxide layer, shows high activity in

catalyzing the reduction of I_3^- in electrolyte. CNT also shows superior catalytic activity derived from numerous defect-rich sites besides high electrical conductivity and large surface area. A lot of reports exhibit comparable or even better photoelectric performances of CNT-based solar cells compared with platinum-based devices.¹⁰⁹⁻¹¹³

The structure of CNTs plays a critical role on the performance of the resulting solar cell. Huang and co-workers have compared the DSCs with single-walled (diameter <2 nm, length 5-15 μm), double-walled (diameter <5 nm, length <20 μm) and multi-walled (diameter 20-40 nm, length 5-15 μm) CNTs as counter electrodes.¹¹¹ The resulting solar cells based on single, double and multi-walled CNT counter electrodes showed PCEs of 7.61%, 8.03% and 7.06%, respectively. Therefore, the double-walled CNT displayed the best catalytic performance. As a control, the platinum counter electrode-based device showed a PCE of 8.49%, just slightly higher than the double-walled CNT.

Although double-walled CNTs demonstrate higher catalytic activity for the reduction of I_3^- , multi-walled CNTs are more widely used in the counter electrodes of DSCs due to simpler preparations and lower costs (the single-walled CNT also shows a high cost). A lot of efforts are further made to modify the multi-walled CNTs for better catalytic activities.¹¹² Bamboo-like multi-walled CNTs with defect-rich edge planes and lower charge-transport resistances exhibited a PCE of 7.67%, comparable to 7.83% based on a platinum counter electrode.

For the randomly dispersed CNT networks, there are numerous boundaries which produce large contact resistances during charge transport and increase the series resistance of the device. In addition, the surfactants are generally required to improve the dispersion of CNTs in solvents, which further increases the resistances of CNT films.⁹² To this end, aligned CNT films derived from spinable CNT arrays may provide a viable solution to this problem.¹⁰⁹ The aligned CNT-based dye-sensitized solar cell showed a PCE of 4.18%, higher than 3.24% of the random CNT film. After optimization, the PCE of the aligned CNT sheet can be further improved to 6.60%, even higher than 5.27% of the platinum counter electrode. Besides aligned CNT sheets, aligned CNT films prepared by pressing vertical aligned CNT arrays along one direction had been also used as counter electrodes (Fig. 9a and b).¹¹⁰ The electrical conductivities of the resulting film at normal direction and in plane were 10^4 and 10^2 S cm^{-1} , respectively. A high PCE of 8.46% was achieved and much exceeded the platinum (7.32%) (Fig. 9c and d).

3.1.3. Conducting carbon nanotube network

As previously mentioned, the photoanode plays a key role in the light absorption, charge collection and diffusion in DSCs. TiO_2 and ZnO are most explored with large bandgap (3.0-3.2 eV) only in response to ultraviolet light. Therefore, photosensitive dyes are needed as sensitizers to increase the absorption in visible region. To increase the uptake of dyes, porous films are constructed for large specific surface areas. Based on the similar strategy, many labs had tried to use CNTs as photoanode materials in replacement of metal oxides, but the PCEs are much lower than the conventional TiO_2 or ZnO .^{114,115} However, the advantage of rapid charge transport along the length enables the CNT as promising reinforced moieties to improve the charge transport across the network of metal oxide such as TiO_2 .¹¹⁶⁻¹¹⁹

A sol-gel process represents a general method in preparation of TiO_2/CNT hybrid photoanodes.¹¹⁶ The introduction of CNTs had been found to enhance the roughness factor of the electrode from 834 to 1267 and charge recombination, which was beneficial for dye adsorption for high photocurrent. The PCEs were increased with the increasing CNT content, and the optimal CNT weight percentage of 0.3% produced a PCE of 4.62%, higher than 2.87% without CNTs. However, the PCE started to reduce with the further increase of CNT, e.g., 4.22% at the CNT weight percentage of 0.5, mainly due to the decreased short-circuit current that may be resulted by a competing light absorption between CNT and dye.

Although CNTs are studied as a promising material to improve the photoanode, a poor dispersion of CNTs in TiO_2 -based matrix is a big challenge. To this end, the pre-treatment of CNTs are made to improve the dispersion. For instance, both O_2 plasma-treated and chemically modified CNTs were incorporated within a TiO_2 matrix as photoanodes.¹¹⁹ The former showed more uniform holes and rougher surfaces for higher dye adsorption and lower charge recombination (Fig. 10). As a result, the O_2 plasma-treated CNT/TiO_2 based photoanode exhibited a PCE of 6.34%, compared with 4.66% and 3.63% of the chemically modified CNTs and pristine TiO_2 , respectively.

Apart from the pre-treatment, the assembly of CNT and metal oxide can be also used to optimize the structure. The multi-walled CNT had been introduced inside TiO_2 nanorods to perform as ideal electron transport “superhighway”.¹²⁰ At a weight percentage of 0.1%, a high fill factor of 0.74 was achieved to offer a remarkable PCE of 10.24%. This structure design provided a general and effective method for developing photoanodes with high charge transports.

3.1.4. Carbon nanotube/polymer composite

CNTs have been introduced to enhance the PCE and duration of polymer solar cells.¹²¹ The large specific surface area offers a suitable microscopic morphology for exciton dissociation, while the high aspect ratio with high electrical conductivity create percolation pathways for high carrier mobility and rapid charge transport to decrease the recombination, even at low doping levels. Kymakis and Amaratunga incorporated single-walled CNTs into the bulk heterojunction of polymer solar cells.¹²² At a low CNT concentration of below 1%, the resulting polymer solar cell display open-circuit voltages of 0.7–0.9 V. Compared with the bare polymer, the short-circuit current with the use of CNTs was increased by two orders of magnitude, and the fill factor had been also increased from 0.3 to 0.4. The photo-induced electron transfer at the polymer/CNT interface was considered to be the main reason for the above improvement.

Note that semiconducting single-walled CNTs with an n-type character favor the charge transport and have been more widely explored for polymer solar cells.¹²³ A lot of efforts are mainly made to overcome the dispersion problem of CNTs. For example, a rapid charge transport was realized in a heterojunction comprising orientated millimeter-long, single-walled CNTs beneath a poly(3-hexylthiophene) layer (Fig. 11a).¹²⁴ The maximal PCE for one CNT was calculated to be 3.82% (Fig. 11b), which were 50 to 100 times higher than a blend of poly(3-hexylthiophene) and single-walled CNTs. In addition, a covalent functionalization of the ends and defects of CNTs with thiophene moieties can also increase their dispersion in poly(3-octylthiophene) matrix for a much improved performance.¹²⁵

PEDOT:PSS, the most commonly used hole extraction material, suffers from a short lifetime due to the humidity sensitivity and acidity, which cause the degradation of the active layer and ITO electrode. Increasing interests are attracted to develop efficient candidates to replace it. Among them, CNT-modified materials represent one of the most studied systems.^{126,127} For instance, transparent, highly percolated networks composed of region-regular P3HT-wrapped semiconducting single-walled CNTs served as the hole extraction layer to offer a PCE of 7.63%.¹²⁶ As a comparison, a control device based on the PEDOT:PSS hole extraction layer demonstrated a PCE of 7.33% under the same condition.

3.2. Carbon nanofiber

Carbon nanofibers resemble carbon nanotubes in the one-dimensional configuration.¹²⁸ Carbon nanofibers show different diameters and lengths ranging from 10-500 nm and 0.5-100 μm , respectively. Previously, arc-discharge and laser-ablation methods have been developed to synthesize a mixture of carbon nanomaterials that needed

complex purifications to obtain carbon nanofibers. Later, chemical vapor deposition was used to make pure carbon nanofibers aiming to practical applications.¹²⁹ Metal nanoparticles including iron, cobalt and nickel were used to dissolve carbon and form carbides.¹³⁰ A wide variety of precursors such as methane, carbon monoxide, ethyne and ethylene had been used as carbon sources at a temperature range of 700-1200 °C.^{118, 129, 131} Electrospun polymer nanofibers such as polyacrylonitrile (PAN) and pitches can be also carbonized to synthesize carbon nanofibers, whose properties largely depended on the types of polymer solution and processing parameters.^{132,133}

Direct measurements of mechanical properties of individual carbon nanofibers remain unavailable yet. As the ancestor of carbon nanofiber, the vapor-grown carbon fiber shows tensile strength and modulus of 2.9 GPa and 240 GPa, respectively. The electrical resistance of carbon nanofiber grown at 1100 °C was measured to be $2 \times 10^{-3} \Omega \text{ cm}^{-1}$ and had been further decreased to $5 \times 10^{-5} \Omega \text{ cm}^{-1}$ after graphitization.¹³⁴ Currently, due to the low longitudinal resistance, carbon nanofibers have been mainly explored as counter electrodes and photoanodes in DSCs.

3.2.1 Electrocatalytic carbon nanofiber film

Similar to CNTs, carbon nanofibers are mainly investigated as low-cost counter electrodes in DSCs. Electrospun carbon nanofibers produced a DSC that displayed a PCE of 5.5%, much lower than 6.97% based on the platinum counter electrode.¹³⁵ This difference can be attributed to a much higher series resistance of $15.5 \Omega \text{ cm}^2$ in the carbon nanofiber compared with $4.8 \Omega \text{ cm}^2$ of platinum, which produced a much lower fill factor. Based on the above phenomenon, a great improvement had been realized by incorporating platinum nanoparticles onto carbon nanofibers to reduce the series resistance to $3.16 \Omega \text{ cm}^2$.¹³⁶ A much increased PCE of ~8% was achieved.

Although exciting achievements have been made, several problems came up associated with electrospun carbon nanofibers. The required high temperature (700-1200 °C) during carbonization is harsh to most substrates; the transfer process increases the complicity and may cause contamination or damage of carbon nanofibers;^{136,137} the random orientation of carbon nanofibers is a potential obstacle hindering fast charge separation and transport in the counter electrode. To solve the above problems, vertically aligned carbon nanofibers were synthesized at low temperatures.¹³⁸ The series resistance of $29.74 \Omega \text{ cm}^2$ in the vertically aligned carbon nanofiber-based counter electrode was comparable to $25.36 \Omega \text{ cm}^2$ of platinum-based counter electrode. However, rare studies are available to investigate their potentials as counter electrodes.

3.2.2. Conducting carbon nanofiber network

The low electrical resistance along the length direction has also enabled carbon nanofibers to be a promising candidate for the fabrication of high performance photoanode. Li and co-workers synthesized a vertically aligned carbon nanofiber array on a nanoneedle-textured anatase TiO₂ film as effective photoanode (Fig. 12).¹³⁹ A rapid charge separation was achieved at the TiO₂-carbon nanofiber interface, resulting in a relatively low while encouraging PCE of ~1.09%.

For the future application of carbon nanofibers in DSCs, particularly as counter electrodes, the increase in PCE and decrease in cost become two of the most important directions. Although the highest PCE of carbon nanofiber-based DSCs have exceeded 8%, which is comparable to the platinum-based DSCs, it is still lower than CNT-based DSCs. A general and effective route to enhance the PCE may lie in the incorporation of other materials such as platinum nanoparticles. The synthesis of carbon nanofibers requires high temperature and complex process, which are unfavorable for scale-up applications. The high cost of carbon nanofiber, especially compared with its counterparts of platinum and CNT, will be also an obstacle to practical applications. More efforts should be made to develop new synthetic methods to make carbon nanofibers under mild conditions.

4. One-dimensional polymer nanomaterial

The molecular structures of representative conducting polymers are shown in Fig. 13, including polypyrrole (PPy), polyaniline (PANI), polythiophene (PTh) and poly(p-phenylenevinylene) (PPV). By varying the dopants and doping levels, the conductivities of above polymers can be changed from insulators to semiconductors. Assembling conducting polymers into one-dimensional configuration enables attractive advantages including high conductivity, good electrochemical activity, large specific surface area, short and direct pathways for charge transport, which increases the photovoltaic performance of resulting solar cells.

4.1. Synthesis of one-dimensional conducting polymer

4.1.1. Template-based method

Template method has been widely explored for various kinds of one-dimensional nanomaterials including metal, organic semiconductors and functional composites.¹⁴⁰ In the case of conducting polymers, two main templates can be used during synthesis, i.e., hard and soft templates. In a hard template method, porous membrane materials

such as anodic aluminum oxide, particle track-etched membrane and titanium dioxide nanotube array containing massive micro/nanopores are the most explored templates. For instance, a variety of morphologies including nanorods, nanofibers and nanotubes of conducting polymers such as PPy, PANI, PTh, PEDOT and their derivatives had been synthesized by chemical/electrochemical polymerization using these templates.¹⁴¹⁻¹⁴⁴ In a typical synthesis, monomer solutions are penetrated into the pores or coated around the surfaces of templates, and the resulting polymerizations take place in the channels. The uniform and aligned pores of hard templates offer an efficient approach to control the morphology and orientation of polymers. In addition, due to the good stability of hard templates, the sizes of one-dimensional conducting polymers can also be easily tailored in various synthetic conditions such as a wide range of reaction temperature, time and concentration.

Soft templates are generally made from highly ordered aggregates that have been formed by assembling amphiphilic molecules through hydrophilic-hydrophobic interactions, hydrogen bonds, or van der Waals forces when their concentrations reach the critical micelle concentrations. Surfactants, liquid crystals and amphiphilic copolymers can be all used to prepare micelles or reversed micelles in solutions to guide the in situ polymerization and growth of conducting polymers based on the nanostructured soft-templated micelles. After removing the soft templates, conducting polymer nanorods, nanofibers or nanotubes are readily prepared. Similar to the hard templates, the morphology and aspect ratio of the conducting polymer are determined by the assembled micelles that are tunable during preparation.

Despite of many advantages, the template methods also suffer from complicated preparation processes and harsh post-treatments to remove the templates, which may result in damages of conducting polymers. In addition, it remains challenging to scale up with low costs. Furthermore, the introduced impurities are detrimental to the intrinsic properties of conducting polymers. Alternately, some template-free methods have been also extensively investigated to overcome the above shortcomings.

4.1.2. Template-free method

Two main template-free processes are based on self-assembly and electrospinning. Self-assembly has been realized by weak interactions among building blocks such as π - π stacking, dipole-dipole, hydrophobic, van der Waals, hydrogen bonding, electrostatic and ion-dipole interactions to spontaneously form oriented structures. Through this method, one-dimensional nanostructured conducting polymers including PPy, PANI, PEDOT and their functionalized derivatives have been successfully synthesized.^{145,146} For the electrospinning method, the basic equipment consists of

three main parts: a high-voltage power supply, a spinneret and an electrical conductive collector. A high electrical field is applied between conducting polymer fluid containing a syringe with capillary tip and conductive collection drum to prepare continuous nanofibers. The applied electrical field should be high enough to allow the electrostatic force to overcome the surface tension of the polymer solution, after which a liquid jet forms and moves towards the conductive collection electrode. With the movement of the liquid jet, the solvent evaporates (or the melt solidifies) and the polymer nanofibers are collected on the collector surface. The morphology and size of the nanofibers are controlled by the voltage applied, viscosity, concentration, conductivity of solution, solution surface tension and distance and direction between the nozzle and the collector. Compared with the template-based synthesis and self-assembly, electrospinning is favorable for preparing nanofibers with high aspect ratios and aligned polymer nanofiber films. Therefore, electrospinning has been widely used to prepare nanofibers or nanocables of conducting polymers and their composites.¹⁴⁷ For instance, electrospinning was used to prepare (poly[N-9'-hepta-decanyl-2,7-carbazole-alt-5,5-(4',7'-di-2-thienyl-2',1',3'-benzothiazole)]) nanofibers for polymer solar cells.¹⁴⁸ The nanofiber active layer exhibited 100% photoluminescence quenching due to small diameters of nanofibers, indicating an efficient dissociation of excitons.

4.2. Representative conducting polymer

4.2.1. Polypyrrole

Polypyrrole (PPy) has been widely investigated due to high electronic conductivity, biocompatibility and stability in both air and aqueous media.¹⁴⁹ For instance, PPy nanorod networks synthesized through electrochemical polymerization exhibited a high electrical conductivity of 40 S cm^{-1} that enables efficient counter electrode for dye-sensitized solar cell (Fig. 14). The electrocatalytic performance could be further enhanced by incorporating carbon nanoparticles. After introduction of 10 wt% carbon nanoparticles, a reduced charge transport resistance and improved catalytic performance for the reduction of I_3^- to I^- has been achieved, and the interaction between PPy nanorod networks and carbon nanoparticles accelerated the electron transport at the counter electrode. The resulting dye-sensitized solar cells displayed a PCE of 7.2%.¹⁵⁰

4.2.2. Polyaniline

Polyaniline (PANI) has been also employed as counter electrodes for dye-sensitized solar cells due to a remarkable electrocatalytic activity.^{151,152} It typically appears in a

bulk material in the use of solar cells. However, for a bulk form, the slow charge transport and low electrolyte penetration decrease its performance during use. To this end, the formation of PANI nanomaterials offers large specific surface area and porosity, and the one-dimensional configuration is particularly promising for a rapid charge transport during photovoltaic conversion. As a result, PANI nanofibers have been investigated as high-performance counter electrodes, and a PCE of 6.58% was achieved and can be further largely increased after optimization.^{153,154}

4.2.3. Poly (3,4-ethylenedioxythiophene)

Bulk PEDOT has been also used as counter electrodes for dye-sensitized solar cells, and one-dimensional PEDOT nanomaterials were mostly demonstrated as high performances electrocatalyst.^{155,156} For instance, PEDOT nanofibers with diameters of 10-50 nm and high electrical conductivity (up to 83 S cm⁻¹) synthesized by soft-template methods produced a PCE of 9.2%, much higher than 6.8% based on a bulk PEDOT counter electrode and even higher than 8.6% of the conventional platinum.¹⁵⁷ It was shown that PEDOT nanofibers could efficiently reduce I₃⁻ ions to enhance both current density and fill factor.

Apart from the application in dye-sensitized solar cells, PEDOT can also serve as a viable hole extracting material in polymer solar cells. For a network from PEDOT nanofibers, the formed porous structure offered a high interface to enhance both hole extraction and transport.¹⁵⁸ The PEDOT nanofiber-modified ITO electrode was incorporated with spin-coated P3HT-PCBM photoactive layer to fabricate polymer solar cells without annealing. Compared with the conventional spin-coated PEDOT-PSS at the same thickness, although the open-circuit voltage and short-circuit current were the same, a 30% improvement in the fill factor was observed for PEDOT nanofibers. This phenomenon was attributed to higher hole extraction and transport in PEDOT nanofibers and better contacts with ITO electrode and photoactive layer.¹⁵⁹

4.2.4. Polythiophene and derivatives

Unlike the conducting polymers discussed above, polythiophene (PTh) and its derivatives are usually used as the photoactive layer to absorb photon in polymer solar cells. The semiconducting polymers absorb light for charge generation and separation at the interface with electrode buffer layers. To fabricate high performance polymer solar cells, the morphology of photoactive layer containing semiconducting polymers is a critical factor. There are numerous reports focusing on the optimization of this bulk heterojunction layer containing polymer donor and acceptor to form a suitable micro-phase separation, which enhanced the carrier transport and favored high current

density and fill factor.^{160,161} An effective route to enhance the photoelectric performance of bulk heterojunction device lies in the use of nanofiber networks that increase the charge separation and transport.¹⁶²

To better understand the enhancement of polymer solar cells with active nanofiber network layers, Sum et al. investigated the charge generation and recombination dynamics in P3HT-nanofiber using transient absorption spectroscopy. The spectra showed a more efficient charge generation in the nanofiber network compared with the control bulk samples. However, there was also a significant amount of non-geminate recombination in the nanofiber network, which may reduce open-circuit voltage and short-circuit current density.¹⁶³ To increase the charge transport and decrease charge localization, external electric field treatment of the active layer was conducted to align the randomly dispersed polymer chains to be perpendicular to the electrode. A 22.7% improvement in PEC and 37.5% improvement in charge mobility had been achieved after the treatment.¹⁶⁴

5. One-dimensional nanomaterials for one-dimensional solar cells

Attributed to the unique advantages including flexibility, light weight and weavability, one-dimensional solar cells have attracted intense attentions in the past decade. Various kinds of solar cells including dye-sensitized solar cells, polymer solar cells and perovskite solar cells have been developed with satisfactory performances. One-dimensional fiber electrodes are the heart of the one-dimensional solar cells and the mechanical and electrical properties of the fiber electrode plays a critical role on the photovoltaic performances. At the early stage, metal wires including stainless steel wires, platinum wires and titanium wires are widely explored.¹⁶⁵ However, the relatively low flexibility and high weight of the metal wires have limited their practical applications. For some noble metal wires such as platinum wires, the high cost during fabrication cannot be ignored either. To this end, aligned CNT fiber assembled from numerous CNTs provides an effective solution (Fig. 15a).¹⁶⁶ In this section, the applications of aligned CNT materials, mainly CNT fibers, are briefly described for one-dimensional solar cells.

Aligned CNT fibers are generally drawn from spinnable CNT arrays which are synthesized via chemical vapor deposition.^{92, 167, 168} The obtained CNT fibers show high tensile strengths on the level of 10^2 - 10^3 MPa and electrical conductivities at the order of 10^2 - 10^3 S cm^{-1} . Aligned CNT fibers were firstly used as photoanodes to fabricate planar DSCs.¹¹⁴ An aligned CNT fiber was incorporated with dye molecules through a solution process in replacement of TiO_2 . The resulting planar dye-sensitized solar cell showed PCEs ranged from 2.1% to 2.6%. Later, aligned CNT fibers were

used to replace metal wires as the photoanodes to support dye-loaded TiO₂ nanoparticles with another aligned CNT fiber serving as the counter electrode to produce a one-dimensional DSC (Fig. 15d).¹⁶⁶ The PCE achieved 2.94%. Basically, the relatively low conductivity in CNT fiber is not favorable for photoanodes aiming at highly efficient solar cells. Alternately, more efforts have been made to develop CNT fibers for efficient counter electrodes in reduction of I₃⁻ ions in DSCs.¹⁶⁹ For instance, an aligned CNT fiber was twisted onto a titanium wire perpendicularly grown with aligned titanium dioxide nanotubes on the outer surface, which served as the photoanode of the DSC (Fig. 15b and c). After optimization, the PCE of the resulting one-dimensional solar cell achieved 4.6%, which was also independent of the angle of incident light due to the unique one-dimensional configuration in the device. Currently, a lot of investigations have been made to improve the PCE^{170,171} and stability^{172,173} and introduce more functionalities^{113,174,175} of the CNT fiber-based one-dimensional dye-sensitized solar cells. The maximal PCE reported to date is 8.50% based on a liquid electrolyte.¹⁷¹ For most reports, the one-dimensional dye-sensitized solar cells are fabricated from liquid electrolytes, and some solid electrolytes have been also tried but with much lower PCEs.

Aligned CNT fibers have also been used to fabricate one-dimensional polymer solar cells. For instance, aligned CNT fiber and aligned TiO₂ nanotube-modified Ti wire as two electrodes were twisted into a fiber-shaped polymer solar cell.¹⁷⁶ By filling the TiO₂ nanotubes with active polymer layer, efficient exciton separation and electron transport were realized to produce efficient polymer solar cells that showed a PCE of 1.8%.¹⁷⁷ Although the PCEs are lower than those of DSCs, the all-solid-state one-dimensional polymer solar cells shared a higher stability compared with liquid-electrolyte based DSCs.

As one kind of burgeoning solar cells, perovskite solar cells have attracted a great deal of interest due to an all solid state and high efficiencies, which are particularly promising for the one-dimensional photovoltaic devices aiming at practical applications. Fiber-shaped perovskite solar cells started to attract attentions just in recent years, and an attempt was successfully made by using CNT sheets as transparent electrode and aligned TiO₂ nanotubes as electron transporting layer with a coaxial structure (Fig. 16).¹⁷⁸ This perovskite solar cell displayed a PCE of 3.5% that is currently acceptable but obviously much lower than the planar counterparts. A lot of efforts should be made to optimize it for a higher PCE.

Although encouraging achievements have been made using aligned CNT sheets or fibers as efficient electrodes in fabrication of one-dimensional solar cells, the PCEs are still lower than the conventional planar devices, particularly for polymer and

perovskite solar cells. To overcome this dilemma, more efforts should be made to further enhance the electrical conductivity of aligned CNT electrode materials to significantly improve both charge transport and collection, which may reduce the series resistance of the resulting devices. In addition, a second active phase including the other one-dimensional inorganic nanomaterials and conducting polymers may be also incorporated into aligned CNT fibers for higher catalytic capability.

6. Conclusion and prospective

The birth and burgeoning of dye-sensitized and polymer solar cells have renewed the interest in photovoltaics in the past two decades. Recently, the new recruit, perovskite solar cell which has boosted a staggering increase in performance, rejuvenate the race in harnessing the sunlight. It is often the case that the upgrade in performance is always accompanied by the innovation in materials. One-dimensional materials, benefiting from its geometry configuration, stand out as promising candidates. Metal, metal oxide, carbonaceous material and conducting polymer have been all made into a one-dimensional configuration spanning from nanowire, nanofiber, nanorod to nanotube that are carefully described for photovoltaic applications in this review. Inheriting the intrinsic properties from these materials, the one-dimensional configuration introduces several advantages like efficient charge transport and collection, which contributes to a better photovoltaic performance. As a penalty, the one-dimensional configuration imposes a restriction on the specific surface area, which is detrimental to uptake of active materials. Fortunately, it can be offset by the designed hierarchical structures. Moreover, the one-dimensional carbonaceous materials including carbon nanofibers and carbon nanotubes can assemble into a one-dimensional yarn that is favorable for fiber-shaped solar cells.

The one-dimensional materials have been widely appreciated in their applications in solar cells. Looking forwards into the future, there are still substantial opportunities in many directions. Some of them are summarized below: (1) Synthesizing new one-dimensional nanomaterials or modifying existing species to further improve the electronic properties for better photovoltaic performances. (2) Developing and enriching the synthetic methods of one-dimensional nanomaterials, and clarifying synthetic factors to accurately control the morphology and properties of the resulting materials in order to steadily fabricate high-performance photovoltaic devices. (3) Simplifying the fabrication process and reducing the fabrication cost. The present methods for the synthesis of one-dimensional nanomaterials are generally based on chemical vapor deposition, hydrothermal method or anodic oxidation which requires rigorous conditions or specific equipment. Considering the practical applications of solar cells, it is critically important to simplify the fabrication process and reduce the

fabrication cost of one-dimensional nanomaterials, which calls for deep investigation and exploration in the future. (4) Fiber-shaped solar cells have recently attracted increasing attentions and are proposed to power various portable and wearable electronic products, therefore changing the modern life. The one-dimensional nanomaterials are found to be promising candidates for fiber electrodes, a key part to achieve both high PCE and stability, due to combined high flexibility and electronic property on the basis of aligned nanostructures. A lot of efforts can be made along this direction to push the fiber-shaped solar cells forward.

Acknowledgements

This work was supported by MOST (2011CB932503), NSFC (21225417), STCSM (12nm0503200), the Fok Ying Tong Education Foundation, the Program for Special Appointments of Professors at Shanghai Institutions of Higher Learning, and the Program for Outstanding Young Scholars from the Organization Department of the CPC Central Committee.

References

- 1 M. He, W. Han, J. Ge, Y. Yang, F. Qiu, Z. Lin, *Energy Environ. Sci.* **2011**, *4*, 2894-2902.
- 2 M. He, F. Qiu, Z. Lin, *J. Mater. Chem.* **2011**, *21*, 17039-17048.
- 3 M. He, F. Qiu, Z. Lin, *J. Phys. Chem. Lett.* **2013**, *4*, 1788-1796.
- 4 N. Robertson, *Angew. Chem. Int. Ed.* **2006**, *45*, 2338-2345.
- 5 M. Gratzel, *Acc. Chem. Res.* **2009**, *42*, 1788-1798.
- 6 A. Hagfeldt, G. Boschloo, L. C. Sun, L. Kloo, H. Pettersson, *Chem. Rev.* **2010**, *110*, 6595-6663.
- 7 F.-C. Chen, H.-C. Tseng, C.-J. Ko, *Appl. Phys. Lett.* **2008**, *92*, 103316.
- 8 F.-C. Chen, C.-J. Ko, J.-L. Wu, W.-C. Chen, *Sol. Energy Mater. Sol. Cells* **2010**, *94*, 2426-2430.
- 9 C. R. McNeill, *Energy Environ. Sci.* **2012**, *5*, 5653-5667.
- 10 Y. Liu, J. Zhao, Z. Li, C. Mu, W. Ma, H. Hu, K. Jiang, H. Lin, H. Ade, H. Yan, *Nature Comm.* **2014**, *5*, 5293.
- 11 V. D'Innocenzo, G. Grancini, M. J. P. Alcocer, A. R. S. Kandada, S. D. Stranks, M. M. Lee, G. Lanzani, H. J. Snaith, A. Petrozza, *Nature Comm.* **2014**, *5*, 3586.
- 12 Q. Lin, A. Armin, R. C. R. Nagiri, P. L. Burn, P. Meredith, *Nature Photon.* **2014**, doi:10.1038/nphoton.2014.284.
- 13 M. Song, D. S. You, K. Lim, S. Park, S. Jung, C. S. Kim, D. H. Kim, D. G. Kim, J. K. Kim, J. Park, *Adv. Funct. Mater.* **2013**, *23*, 4177-4184.
- 14 L. Hu, H. S. Kim, J.-Y. Lee, P. Peumans, Y. Cui, *ACS Nano* **2010**, *4*, 2955-2963.
- 15 Z. He, H. Phan, J. Liu, T. Q. Nguyen, T. T. Tan, *Adv. Mater.* **2013**, *25*, 6900-6904.
- 16 H. J. Snaith, L. Schmidt-Mende, *Adv. Mater.* **2007**, *19*, 3187-3200.
- 17 J. H. Yum, P. Chen, M. Gratzel, M. K. Nazeeruddin, *ChemSusChem* **2008**, *1*, 699-707.
- 18 X. Sun, T. Chen, Z. Yang, H. Peng, *Acc. Chem. Res.* **2013**, *46*, 539-549.
- 19 A. Kim, Y. Won, K. Woo, C.-H. Kim, J. Moon, *ACS Nano* **2013**, *7*, 1081-1091.
- 20 S.-E. Park, S. Kim, D.-Y. Lee, E. Kim, J. Hwang, *J. Mater. Chem. A* **2013**, *1*, 14286-14293.
- 21 J.-Y. Wang, S.-Y. Yang, Y.-L. Huang, H.-W. Tien, W.-K. Chin, C.-C. M. Ma, *J. Mater. Chem.* **2011**, *21*, 13569-13575.
- 22 J.-W. Lim, D.-Y. Cho, K. Eun, S.-H. Choa, S.-I. Na, J. Kim, H.-K. Kim, *Sol. Energy Mater. Sol. Cells* **2012**, *105*, 69-76.
- 23 G. Y. Margulis, M. G. Christoforo, D. Lam, Z. M. Beiley, A. R. Bowring, C. D. Bailie, A. Salleo, M. D. McGehee, *Adv. Energy Mater.* **2013**, *3*, 1657-1663.
- 24 C.-H. Kim, S.-H. Cha, S. C. Kim, M. Song, J. Lee, W. S. Shin, S.-J. Moon, J. H. Bahng, N. A. Kotov, S.-H. Jin, *ACS Nano* **2011**, *5*, 3319-3325.
- 25 M. G. Kang, T. Xu, H. J. Park, X. Luo, L. J. Guo, *Adv. Mater.* **2010**, *22*, 4378-4383.
- 26 A. R. Rathmell, S. M. Bergin, Y. L. Hua, Z. Y. Li, B. J. Wiley, *Adv. Mater.*

- 2010, 22, 3558-3563.
- 27 A. R. Rathmell, B. J. Wiley, *Adv. Mater.* **2011**, 23, 4798-4803.
- 28 M. Jin, G. He, H. Zhang, J. Zeng, Z. Xie, Y. Xia, *Angew. Chem. Int. Ed.* **2011**, 50, 10560-10564.
- 29 J. Ren, Y. Zhang, W. Bai, X. Chen, Z. Zhang, X. Fang, W. Weng, Y. Wang, H. Peng, *Angew. Chem.* **2014**, 53, 7864-7869.
- 30 I. E. Stewart, A. R. Rathmell, L. Yan, S. Ye, P. F. Flowers, W. You, B. J. Wiley, *Nanoscale* **2014**, 6, 5980-5988.
- 31 V. Thavasi, G. Singh, S. Ramakrishna, *Energy Environ. Sci.* **2008**, 1, 205-221.
- 32 L. Yang, W. W. F. Leung, *Adv. Mater.* **2013**, 25, 1792-1795.
- 33 Y. P. Lin, Y. Y. Chen, Y. C. Lee, Y. W. Chen-Yang, *J. Phys. Chem. C* **2012**, 116, 13003-13012.
- 34 E. Ghadiri, N. Taghavinia, S. M. Zakeeruddin, M. Graetzel, J.-E. Moser, *Nano Lett.* **2010**, 10, 1632-1638.
- 35 S. H. Hwang, C. Kim, H. Song, S. Son, J. Jang, *ACS Appl. Mater. Interfaces* **2012**, 4, 5287-5292.
- 36 A. I. Hochbaum, P. Yang, *Chem. Rev.* **2010**, 110, 527-546.
- 37 P. Zhu, A. S. Nair, S. Yang, S. Peng, S. Ramakrishna, *J. Mater. Chem.* **2011**, 21, 12210-12212.
- 38 L. Yang, W. W. F. Leung, *Adv. Mater.* **2011**, 23, 4559-4562.
- 39 S. Dharani, H. K. Mulmudi, N. Yantara, P. T. T. Trang, N. G. Park, M. Graetzel, S. Mhaisalkar, N. Mathews, P. P. Boix, *Nanoscale* **2014**, 6, 1675-1679.
- 40 L. Miao, S. Tanemura, S. Toh, K. Kaneko, M. Tanemura, *J. Cryst. Growth* **2004**, 264, 246-252.
- 41 Y. Li, M. Guo, M. Zhang, X. Wang, *Mater. Res. Bull.* **2009**, 44, 1232-1237.
- 42 J.-M. Wu, H. C. Shih, W.-T. Wu, *Nanotechnology* **2006**, 17, 105-109.
- 43 X. Feng, K. Shankar, O. K. Varghese, M. Paulose, T. J. Latempa, C. A. Grimes, *Nano Lett.* **2008**, 8, 3781-3786.
- 44 B. Liu, E. S. Aydil, *J. Am. Chem. Soc.* **2009**, 131, 3985-3990.
- 45 X. Feng, K. Zhu, A. J. Frank, C. A. Grimes, T. E. Mallouk, *Angew. Chem. Int. Ed.* **2012**, 124, 2781-2784.
- 46 P. Sun, X. Zhang, X. Liu, L. Wang, C. Wang, J. Yang, Y. Liu, *J. Mater. Chem.* **2012**, 22, 6389-6393.
- 47 E. Barea, X. Xu, V. González-Pedro, T. Ripollés-Sanchis, F. Fabregat-Santiago, J. Bisquert, *Energy Environ. Sci.* **2011**, 4, 3414-3419.
- 48 M. Lv, D. Zheng, M. Ye, J. Xiao, W. Guo, Y. Lai, L. Sun, C. Lin, J. Zuo, *Energy Environ. Sci.* **2013**, 6, 1615-1622.
- 49 Q. Huang, G. Zhou, L. Fang, L. Hu, Z.-S. Wang, *Energy Environ. Sci.* **2011**, 4, 2145-2151.
- 50 S. Lee, I. J. Park, D. H. Kim, W. M. Seong, D. W. Kim, G. S. Han, J. Y. Kim, H. S. Jung, K. S. Hong, *Energy Environ. Sci.* **2012**, 5, 7989-7995.
- 51 L.-L. Li, C.-Y. Tsai, H.-P. Wu, C.-C. Chen, E. W.-G. Diau, *J. Mater. Chem.* **2010**, 20, 2753-2758.
- 52 J. Wang, Z. Lin, *Chem. Mater.* **2009**, 22, 579-584.

- 53 M. Ye, D. Zheng, M. Lv, C. Chen, C. Lin, Z. Lin, *Adv. Mater.* **2013**, *25*, 3039-3044.
- 54 M. Ye, X. Xin, C. Lin, Z. Lin, *Nano Lett.* **2011**, *11*, 3214-3220.
- 55 B.-X. Lei, J.-Y. Liao, R. Zhang, J. Wang, C.-Y. Su, D.-B. Kuang, *J. Phys. Chem. C* **2010**, *114*, 15228-15233.
- 56 Q. Chen, D. Xu, *J. Phys. Chem. C* **2009**, *113*, 6310-6314.
- 57 C.-J. Lin, W.-Y. Yu, S.-H. Chien, *J. Mater. Chem.* **2010**, *20*, 1073-1077.
- 58 C.-T. Yip, M. Guo, H. Huang, L. Zhou, Y. Wang, C. Huang, *Nanoscale* **2012**, *4*, 448-450.
- 59 D. K. Roh, W. S. Chi, H. Jeon, S. J. Kim, J. H. Kim, *Adv. Funct. Mater.* **2014**, *24*, 379-386.
- 60 W.-Q. Wu, B.-X. Lei, H.-S. Rao, Y.-F. Xu, Y.-F. Wang, C.-Y. Su, D.-B. Kuang, *Sci. Rep.* **2013**, *3*, 1352.
- 61 L. Chu, L. Li, J. Su, F. Tu, N. Liu, Y. Gao, *Sci. Rep.* **2014**, *4*, 4420.
- 62 J.-Y. Liao, B.-X. Lei, H.-Y. Chen, D.-B. Kuang, C.-Y. Su, *Energy Environ. Sci.* **2012**, *5*, 5750-5757.
- 63 F. Shao, J. Sun, L. Gao, S. Yang, J. Luo, *J. Mater. Chem.* **2012**, *22*, 6824-6830.
- 64 W.-Q. Wu, H.-S. Rao, H.-L. Feng, H.-Y. Chen, D.-B. Kuang, C.-Y. Su, *Nano Energy* **2014**, *9*, 15-24.
- 65 W.-Q. Wu, H.-L. Feng, H.-S. Rao, Y.-F. Xu, D.-B. Kuang, C.-Y. Su, *Nat. Commun.* **2014**, *5*, 3968.
- 66 W.-Q. Wu, Y.-F. Xu, H.-S. Rao, C.-Y. Su, D.-B. Kuang, *J. Am. Chem. Soc.* **2014**, *136*, 6437-6445.
- 67 Q. Zheng, H. Kang, J. Yun, J. Lee, J. H. Park, S. Baik, *ACS Nano* **2011**, *5*, 5088-5093.
- 68 Z. Sun, J. H. Kim, Y. Zhao, D. Attard, S. X. Dou, *Chem. Commun.* **2013**, *49*, 966-968.
- 69 S. C. Lyu, Y. Zhang, C. J. Lee, H. Ruh, H. J. Lee, *Chem. Mater.* **2003**, *15*, 3294-3299.
- 70 H. Dai, Y. Zhou, Q. Liu, Z. Li, C. Bao, T. Yu, Z. Zhou, *Nanoscale* **2012**, *4*, 5454-5460.
- 71 W. Wang, Q. Zhao, H. Li, H. Wu, D. Zou, D. Yu, *Adv. Funct. Mater.* **2012**, *22*, 2775-2782.
- 72 J. Bae, Y. J. Park, M. Lee, S. N. Cha, Y. J. Choi, C. S. Lee, J. M. Kim, Z. L. Wang, *Adv. Mater.* **2011**, *23*, 3446-3449.
- 73 Y. Wei, C. Xu, S. Xu, C. Li, W. Wu, Z. L. Wang, *Nano Lett.* **2010**, *10*, 2092-2096.
- 74 B. Weintraub, Y. Wei, Z. L. Wang, *Angew. Chem. Int. Ed.* **2009**, *121*, 9143-9147.
- 75 C. Xu, J. Wu, U. V. Desai, D. Gao, *J. Am. Chem. Soc.* **2011**, *133*, 8122-8125.
- 76 X. Lan, J. Bai, S. Masala, S. M. Thon, Y. Ren, I. J. Kramer, S. Hoogland, A. Simchi, G. I. Koleilat, D. Paz - Soldan, *Adv. Mater.* **2013**, *25*, 1769-1773.
- 77 J. S. Bendall, L. Etgar, S. C. Tan, N. Cai, P. Wang, S. M. Zakeeruddin, M. Grätzel, M. E. Welland, *Energy Environ. Sci.* **2011**, *4*, 2903-2908.

- 78 N. O. Plank, H. J. Snaith, C. Ducati, J. S. Bendall, L. Schmidt-Mende, M. E. Welland, *Nanotechnology* **2008**, *19*, 465603.
- 79 J. Schrier, D. O. Demchenko, L.-W. Wang, A. P. Alivisatos, *Nano Lett.* **2007**, *7*, 2377-2382.
- 80 N. O. Plank, I. Howard, A. Rao, M. W. Wilson, C. Ducati, R. S. Mane, J. S. Bendall, R. R. Louca, N. C. Greenham, H. Miura, *J. Phys. Chem. C* **2009**, *113*, 18515-18522.
- 81 R. K. Joshi, J. J. Schneider, *Chem. Soc. Rev.* **2012**, *41*, 5285-5312.
- 82 G. Yuan, W. Zhang, J. Jie, X. Fan, J. A. Zapien, Y. H. Leung, L. Luo, P. Wang, C. S. Lee, S. T. Lee, *Nano Lett.* **2008**, *8*, 2591-2597.
- 83 M.-P. Lu, J. Song, M.-Y. Lu, M.-T. Chen, Y. Gao, L.-J. Chen, Z. L. Wang, *Nano Lett.* **2009**, *9*, 1223-1227.
- 84 S. Kim, J. H. Koh, X. Yang, W. S. Chi, C. Park, J. W. Leem, B. Kim, S. Seo, Y. Kim, J. S. Yu, *Adv. Energy Mater.* **2014**, *4*, 1301338.
- 85 D.-Y. Son, J.-H. Im, H.-S. Kim, N.-G. Park, *J. Phys. Chem. C* **2014**, *118*, 16567-16573.
- 86 H.-M. Cheng, W.-H. Chiu, C.-H. Lee, S.-Y. Tsai, W.-F. Hsieh, *J. Phys. Chem. C* **2008**, *112*, 16359-16364.
- 87 S. H. Ko, D. Lee, H. W. Kang, K. H. Nam, J. Y. Yeo, S. J. Hong, C. P. Grigoropoulos, H. J. Sung, *Nano Lett.* **2011**, *11*, 666-671.
- 88 J. Qiu, M. Guo, Y. Feng, X. Wang, *Electrochim. Acta* **2011**, *56*, 5776-5782.
- 89 V.-M. Guéin, T. Pauporté *Energy Environ. Sci.* **2011**, *4*, 2971-2979.
- 90 M. McCune, W. Zhang, Y. Deng, *Nano Lett.* **2012**, *12*, 3656-3662.
- 91 S. Iijima, *Nature* **1991**, *354*, 56-58.
- 92 X. M. Sun, H. Sun, H. P. Li, H. S. Peng, *Adv. Mater.* **2013**, *25*, 5153-5176.
- 93 E. T. Thostenson, Z. F. Ren, T. W. Chou, *Compos. Sci. Technol.* **2001**, *61*, 1899-1912.
- 94 R. H. Baughman, A. A. Zakhidov, W. A. de Heer, *Science* **2002**, *297*, 787-792.
- 95 D. Tasis, N. Tagmatarchis, A. Bianco, M. Prato, *Chem. Rev.* **2006**, *106*, 1105-1136.
- 96 M. F. Yu, O. Lourie, M. J. Dyer, K. Moloni, T. F. Kelly, R. S. Ruoff, *Science* **2000**, *287*, 637-640.
- 97 J. W. G. Wildoer, L. C. Venema, A. G. Rinzler, R. E. Smalley, C. Dekker, *Nature* **1998**, *391*, 59-62.
- 98 S. Hong, S. Myung, *Nat. Nanotechnol.* **2007**, *2*, 207-208.
- 99 K. Kaneto, M. Tsuruta, G. Sakai, W. Y. Cho, Y. Ando, *Synth. Met.* **1999**, *103*, 2543-2546.
- 100 K. Suzuki, M. Yamaguchi, M. Kumagai, S. Yanagida, *Chem. Lett.* **2003**, *32*, 28-29.
- 101 L. J. Brennan, M. T. Byrne, M. Bari, Y. K. Gun'ko, *Adv. Energy Mater.* **2011**, *1*, 472-485.
- 102 C. M. Aguirre, S. Auvray, S. Pigeon, R. Izquierdo, P. Desjardins, R. Martel, *Appl. Phys. Lett.* **2006**, *88*, 183104.
- 103 A. Hirsch, *Angew. Chem. Int. Ed.* **2002**, *41*, 1853-1859.

- 104 B. Dan, G. C. Irvin, M. Pasquali, *ACS Nano* **2009**, *3*, 835-843.
- 105 S. De, P. E. Lyons, S. Sorel, E. M. Doherty, P. J. King, W. J. Blau, P. N. Nirmalraj, J. J. Boland, V. Scardaci, J. Joimel, J. N. Coleman, *ACS Nano* **2009**, *3*, 714-720.
- 106 S. Kim, J. Yim, X. Wang, D. D. C. Bradley, S. Lee, J. C. Demello, *Adv. Funct. Mater.* **2010**, *20*, 2310-2316.
- 107 D. H. Zhang, K. Ryu, X. L. Liu, E. Polikarpov, J. Ly, M. E. Tompson, C. W. Zhou, *Nano Lett.* **2006**, *6*, 1880-1886.
- 108 D. Y. Cho, K. Eun, S. H. Choa, H. K. Kim, *Carbon* **2014**, *66*, 530-538.
- 109 Z. B. Yang, T. Chen, R. X. He, G. Z. Guan, H. P. Li, L. B. Qiu, H. S. Peng, *Adv. Mater.* **2011**, *23*, 5436-5439.
- 110 Z. B. Yang, L. Li, H. J. Lin, Y. F. Luo, R. X. He, L. B. Qiu, J. Ren, H. S. Peng, *Chem. Phys. Lett.* **2012**, *549*, 82-85.
- 111 D. W. Zhang, X. D. Li, S. Chen, Z. Sun, X. J. Yin, S. M. Huang, *Microchim. Acta* **2011**, *174*, 73-79.
- 112 W. J. Lee, E. Ramasamy, D. Y. Lee, J. S. Song, *ACS Appl. Mater. Interfaces* **2009**, *1*, 1145-1149.
- 113 H. Sun, Z. Yang, X. Chen, L. Qiu, X. You, P. Chen, H. Peng, *Angew. Chem. Int. Ed.* **2013**, *125*, 8434-8438.
- 114 T. Chen, S. T. Wang, Z. B. Yang, Q. Y. Feng, X. M. Sun, L. Li, Z. S. Wang, H. S. Peng, *Angew. Chem. Int. Ed.* **2011**, *50*, 1815-1819.
- 115 M. Bissett, A. Barlow, C. Shearer, J. Quinton, J. G. Shapter, *Carbon* **2012**, *50*, 2431-2441.
- 116 C. Y. Yen, Y. F. Lin, S. H. Liao, C. C. Weng, C. C. Huang, Y. H. Hsiao, C. C. M. Ma, M. C. Chang, H. Shao, M. C. Tsai, C. K. Hsieh, C. H. Tsai, F. B. Weng, *Nanotechnology* **2008**, *19*, 375305.
- 117 M. R. Golobostanfard, H. Abdizadeh, *Micropro. Mesopro. Mat.* **2014**, *191*, 74-81.
- 118 A. Kongkanand, R. M. Dominguez, P. V. Kamat, *Nano Lett.* **2007**, *7*, 676-680.
- 119 S. W. Zhang, H. H. Niu, Y. Lan, C. Cheng, J. Z. Xu, X. K. Wang, *J. Phys. Chem. C* **2011**, *115*, 22025-22034.
- 120 L. J. Yang, W. W. F. Leung, *Adv. Mater.* **2013**, *25*, 1792-1795.
- 121 B. Ratier, J. M. Nunzi, M. Aldissi, T. M. Kraft, E. Buncel, *Polym. Int.* **2012**, *61*, 342-354.
- 122 E. Kymakis, G. A. J. Amaratunga, *Appl. Phys. Lett.* **2002**, *80*, 112-114.
- 123 Z. R. Li, V. Saini, E. Dervishi, V. P. Kunets, J. H. Zhang, Y. Xu, A. R. Biris, G. J. Salamo, A. S. Biris, *Appl. Phys. Lett.* **2010**, *96*, 033110.
- 124 M. H. Ham, G. L. C. Paulus, C. Y. Lee, C. Song, K. Kalantar-zadeh, W. Choi, J. H. Han, M. S. Strano, *ACS Nano* **2010**, *4*, 6251-6259.
- 125 A. F. Nogueira, B. S. Lomba, M. A. Soto-Oviedo, C. R. D. Correia, P. Corio, C. A. Furtado, I. A. Hummelgen, *J. Phys. Chem. C* **2007**, *111*, 18431-18438.
- 126 G. Dabera, K. Jayawardena, M. R. R. Prabhath, I. Yahya, Y. Y. Tan, N. A. Nismy, H. Shiozawa, M. Sauer, G. Ruiz-Soria, P. Ayala, V. Stolojan, A. Adikaari, P. D. Jarowski, T. Pichler, S. R. P. Silva, *ACS Nano* **2013**, *7*,

- 556-565.
- 127 S. Chaudhary, H. W. Lu, A. M. Muller, C. J. Bardeen, M. Ozkan, *Nano Lett.* **2007**, *7*, 1973-1979.
- 128 M. Meyyappan, *J. Phys. D. Appl. Phys.* **2009**, *42*, 213001.
- 129 K. P. De Jong, J. W. Geus, *Catal. Rev.* **2000**, *42*, 481-510.
- 130 N. M. Rodriguez, *J. Mater. Res.* **1993**, *8*, 3233-3250.
- 131 G. G. Tibbetts, M. L. Lake, K. L. Strong, B. P. Rice, *Compos. Sci. Technol.* **2007**, *67*, 1709-1718.
- 132 L. C. Feng, N. Xie, J. Zhong, *Materials* **2014**, *7*, 3919-3945.
- 133 S. Cavaliere, S. Subianto, I. Savych, D. J. Jones, J. Roziere, *Energy Environ. Sci.* **2011**, *4*, 4761-4785.
- 134 J. Heremans, *Carbon* **1985**, *23*, 431-436.
- 135 P. Joshi, L. F. Zhang, Q. L. Chen, D. Galipeau, H. Fong, Q. Q. Qiao, *ACS Appl. Mater. Interfaces* **2010**, *2*, 3572-3577.
- 136 P. Poudel, L. F. Zhang, P. Joshi, S. Venkatesan, H. Fong, Q. Q. Qiao, *Nanoscale* **2012**, *4*, 4726-4730.
- 137 P. Joshi, Z. P. Zhou, P. Poudel, A. Thapa, X. F. Wu, Q. Q. Qiao, *Nanoscale* **2012**, *4*, 5659-5664.
- 138 S. M. Mahpeykar, M. K. Tabatabaei, H. Ghafoori-fard, H. Habibiyani, J. Koohsorkhi, *Nanotechnology* **2013**, *24*, 435402.
- 139 J. W. Liu, Y. T. Kuo, K. J. Klabunde, C. Rochford, J. Wu, J. Li, *ACS Appl. Mater. Interfaces* **2009**, *1*, 1645-1649.
- 140 Y. Xia, P. Yang, Y. Sun, Y. Wu, B. Mayers, B. Gates, Y. Yin, F. Kim, H. Yan, *Adv. Mater.* **2003**, *15*, 353-389.
- 141 M. Fu, Y. Zhu, R. Tan, G. Shi, *Adv. Mater.* **2001**, *13*, 1874-1877.
- 142 Y. Cao, T. E. Mallouk, *Chem. Mater.* **2008**, *20*, 5260-5265.
- 143 M. G. Han, S. H. Foulger, *Chem. Commun.* **2005**, 3092-3094.
- 144 S. I. Cho, S. B. Lee, *Acc. Chem. Res.* **2008**, *41*, 699-707.
- 145 M. Wan, *Macromol. Rapid Commun.* **2009**, *30*, 963-975.
- 146 M. Wan, *Adv. Mater.* **2008**, *20*, 2926-2932.
- 147 A. Greiner, J. H. Wendorff, *Angew. Chem. Int. Ed.* **2007**, *46*, 5670-5703.
- 148 T. Kim, S. J. Yang, S. K. Kim, H. S. Choi, C. R. Park, *Nanoscale* **2014**, *6*, 2847-2854.
- 149 A. Fakhry, F. Pillier, C. Debieuvre-Chouvy, *J. Mater. Chem. A* **2014**, *2*, 9859-9865.
- 150 S. Peng, L. Tian, J. Liang, S. G. Mhaisalkar, S. Ramakrishna, *ACS Appl. Mater. Interfaces* **2011**, *4*, 397-404.
- 151 J. Z. Chen, B. Li, J. F. Zheng, J. H. Zhao, H. W. Jing, Z. P. Zhu, *Electrochim. Acta* **2011**, *56*, 4624-4630.
- 152 S. Ameen, M. S. Akhtar, Y. S. Kim, O. B. Yang, H.-S. Shin, *J. Phys. Chem. C* **2010**, *114*, 4760-4764.
- 153 Q. Tang, H. Cai, S. Yuan, X. Wang, *J. Mater. Chem. A* **2013**, *1*, 317-323.
- 154 X. Chen, Q. Tang, B. He, *Mater. Lett.* **2014**, *119*, 28-31.
- 155 L. Zhao, Y. Li, Z. Liu, H. Shimizu, *Chem. Mater.* **2010**, *22*, 5949-5956.

- 156 B. Fan, X. Mei, K. Sun, J. Ouyang, *Appl. Phys. Lett.* **2008**, *93*, 143103.
- 157 T. H. Lee, K. Do, Y. W. Lee, S. S. Jeon, C. Kim, J. Ko, S. S. Im, *J. Mater. Chem.* **2012**, *22*, 21624-21629.
- 158 J. H. Huang, Z. Y. Ho, D. Kekuda, C. W. Chu, K. C. Ho, *J. Phys. Chem. C* **2008**, *112*, 19125-19130.
- 159 E. Nasybulin, S. Wei, M. Cox, I. Kymissis, K. Levon, *J. Phys. Chem. C* **2011**, *115*, 4307-4314.
- 160 K. Maturov \acute{a} S. S. van Bavel, M. M. Wienk, R. A. J. Janssen, M. Kemerink, *Adv. Funct. Mater.* **2011**, *21*, 261-269.
- 161 J. G. Labram, E. B. Domingo, N. Stingelin, D. D. C. Bradley, T. D. Anthopoulos, *Adv. Funct. Mater.* **2011**, *21*, 356-363.
- 162 L. Li, D. L. Jacobs, Y. Che, H. Huang, B. R. Bunes, X. Yang, L. Zang, *Org. Electron.* **2013**, *14*, 1383-1390.
- 163 M. Kurniawan, T. Salim, K. F. Tai, S. Sun, E. J. Sie, X. Wu, E. K. L. Yeow, C. H. A. Huan, Y. M. Lam, T. C. Sum, *J. Phys. Chem. C* **2012**, *116*, 18015-18022.
- 164 A. Solanki, B. Wu, T. Salim, E. K. L. Yeow, Y. M. Lam, T. C. Sum, *J. Phys. Chem. C* **2014**, *118*, 11285-11291.
- 165 T. Chen, L. B. Qiu, Z. B. Yang, H. S. Peng, *Chem. Soc. Rev.* **2013**, *42*, 5031-5041.
- 166 T. Chen, L. B. Qiu, Z. B. Cai, F. Gong, Z. B. Yang, Z. S. Wang, H. S. Peng, *Nano Lett.* **2012**, *12*, 2568-2572.
- 167 G. Z. Sun, Y. N. Zhang, L. X. Zheng, *J. Nanomater.* **2012**, 506209.
- 168 X. F. Zhang, Q. W. Li, T. G. Holesinger, P. N. Arendt, J. Y. Huang, P. D. Kirven, T. G. Clapp, R. F. DePaula, X. Z. Liao, Y. H. Zhao, L. X. Zheng, D. E. Peterson, Y. T. Zhu, *Adv. Mater.* **2007**, *19*, 4198-4201.
- 169 T. Chen, L. B. Qiu, H. G. Kia, Z. B. Yang, H. S. Peng, *Adv. Mater.* **2012**, *24*, 4623-4628.
- 170 S. W. Pan, Z. B. Yang, H. P. Li, L. B. Qiu, H. Sun, H. S. Peng, *J. Am. Chem. Soc.* **2013**, *135*, 10622-10625.
- 171 H. Sun, X. You, J. E. Deng, X. L. Chen, Z. B. Yang, J. Ren, H. S. Peng, *Adv. Mater.* **2014**, *26*, 2868-2873.
- 172 H. P. Li, Z. B. Yang, L. B. Qiu, X. Fang, H. Sun, P. N. Chen, S. W. Pan, H. S. Peng, *J. Mater. Chem. A* **2014**, *2*, 3841-3846.
- 173 H. Sun, H. P. Li, X. You, Z. B. Yang, J. Deng, L. B. Qiu, H. S. Peng, *J. Mater. Chem. A* **2014**, *2*, 345-349.
- 174 H. Sun, X. You, J. Deng, X. L. Chen, Z. B. Yang, P. N. Chen, X. Fang, H. S. Peng, *Angew. Chem. Int. Ed.* **2014**, *53*, 6664-6668.
- 175 Z. Yang, J. Deng, X. Sun, H. Li, H. Peng, *Adv. Mater.* **2014**, *26*, 2643-2647.
- 176 T. Chen, L. Qiu, H. Li, H. Peng, *J. Mater. Chem.* **2012**, *22*, 23655.
- 177 Z. Zhang, Z. Yang, Z. Wu, G. Guan, S. Pan, Y. Zhang, H. Li, J. Deng, B. Sun, H. Peng, *Adv. Energy Mater.* **2014**, *4*, 1301750.
- 178 L. Qiu, J. Deng, X. Lu, Z. Yang, H. Peng, *Angew. Chem. Int. Ed.* **2014**, *53*, 10425-10428.

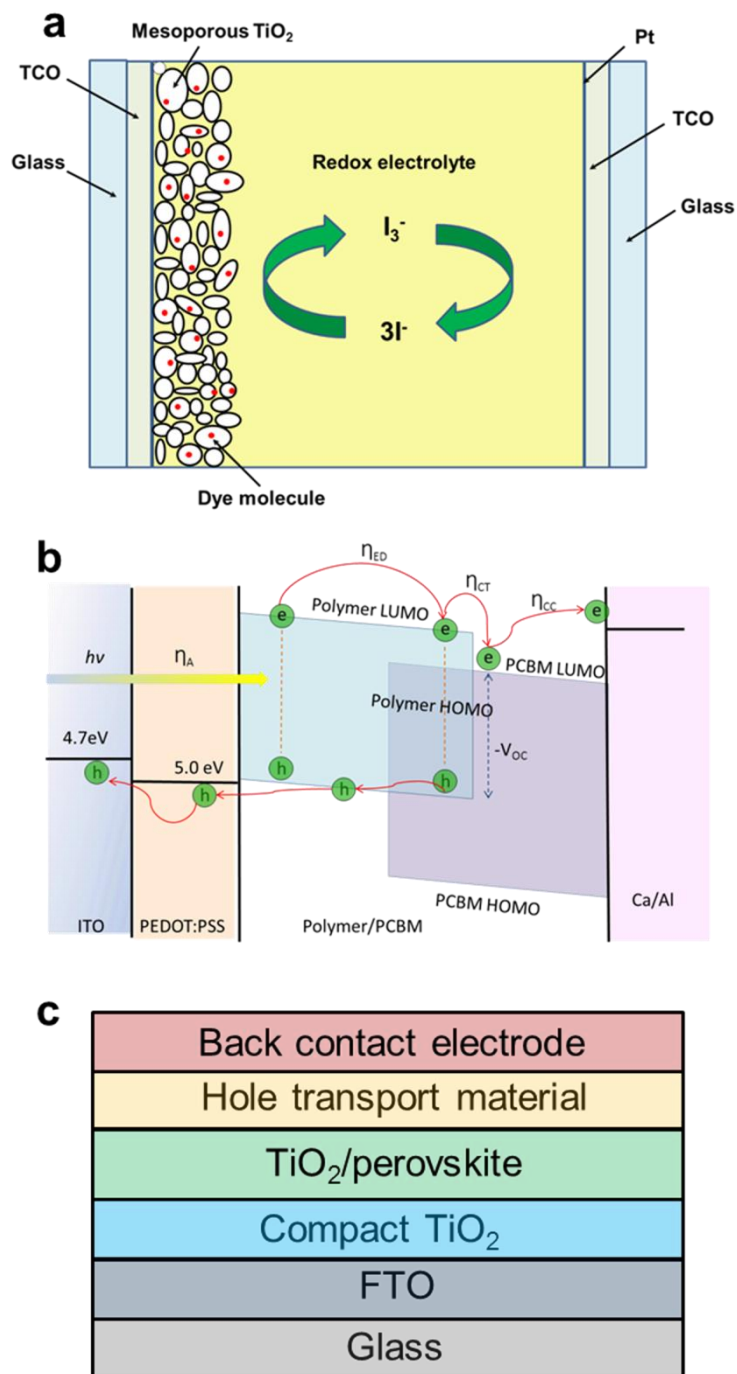


Figure 1. Schematic illustration to the structures of typical (a) dye-sensitized solar cell, (b) polymer solar cell and (c) perovskite solar cell.

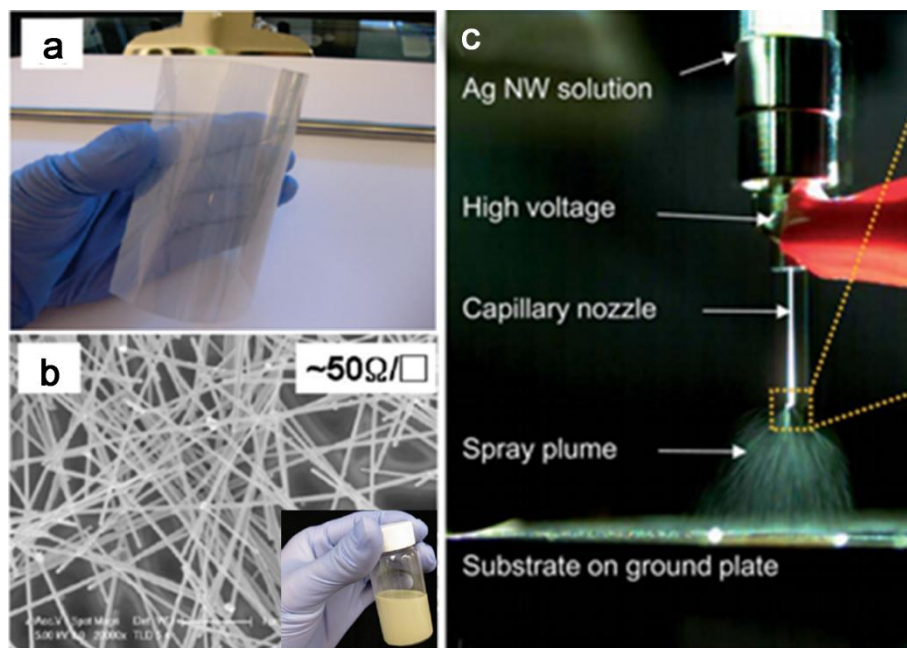


Figure 2. **a.** Ag nanowire film coated on poly (ethylene terephthalate) substrate. **b.** Scanning electron microscope (SEM) image of Ag nanowires (inserted, an Ag nanowire ink in ethanol) (reprinted with permission from ref. 5. Copyright 2010 American Chemical Society). **c.** High-speed camera image of an electrohydrodynamic spray (reprinted with permission from ref. 7. Copyright 2013 Royal Society of Chemistry).

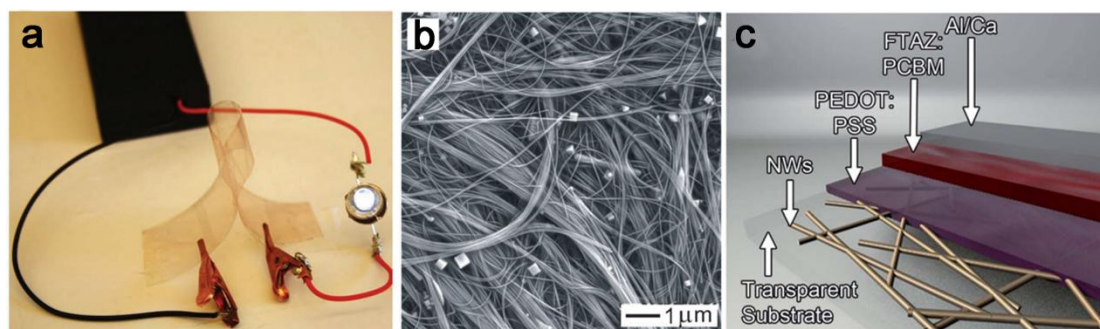


Figure 3. **a.** A bent Cu nanowire film connecting an electrical circuit with a battery pack and a light emitting diode (reprinted with permission from ref. 14. Copyright 2011 Wiley-VCH). **b.** SEM image of Cu nanowires (reprinted with permission from ref. 15. Copyright 2011 Wiley-VCH). **c.** Schematic diagram of the nanowire-based polymer solar cell (reprinted with permission from ref. 17. Copyright 2014 Royal Society of Chemistry).

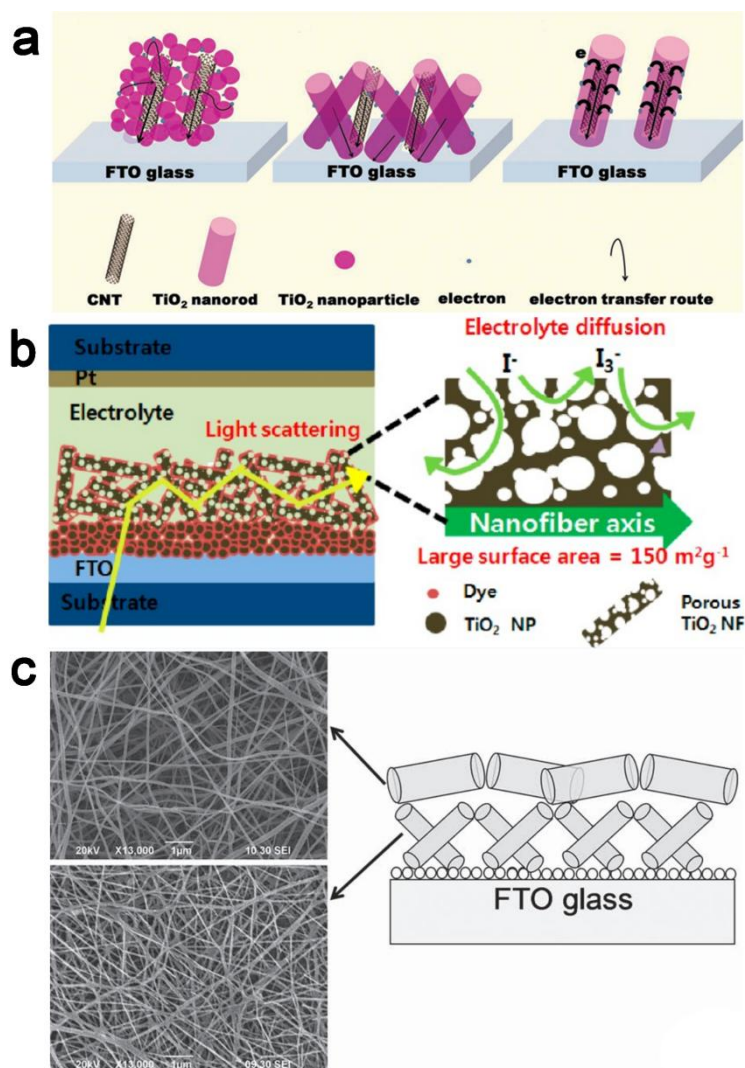


Figure 4. **a.** Mechanism of electron transport across TiO₂ with the assistance of MWCNT (reprinted with permission from ref. 19. Copyright 2013 Wiley-VCH). **b.** Schematic diagrams of dye-sensitized solar cells based on multiscale porous TiO₂ nanofibers (reprinted with permission from ref. 22. Copyright 2012 American Chemical Society). **c.** Schematic diagram of fabrication procedure and SEM images of the bilayer TiO₂ nanofiber photoanode (reprinted with permission from ref. 25. Copyright 2011 Wiley-VCH).

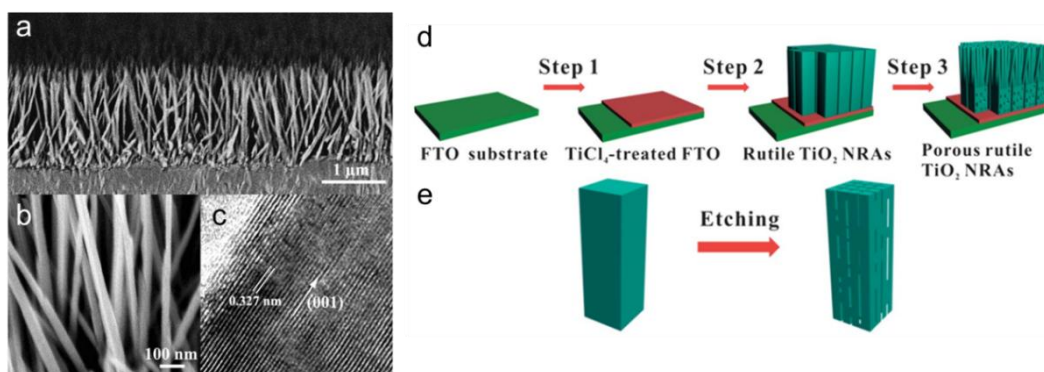


Figure 5. **a, b.** Cross-sectional SEM images of nanowire arrays on FTO-coated glass substrate at low and high magnifications, respectively. **c.** High resolution transmission electron microscopy (TEM) image of the as-synthesized single crystal nanowire (reprinted with permission from ref. 32. Copyright 2012 Wiley-VCH). **d.** Scheme to prepare the porous rutile TiO₂ nanowire array. **e.** Morphological evolution of TiO₂ nanowire by Step 3 (reprinted with permission from ref. 35. Copyright 2013 Royal Society of Chemistry).

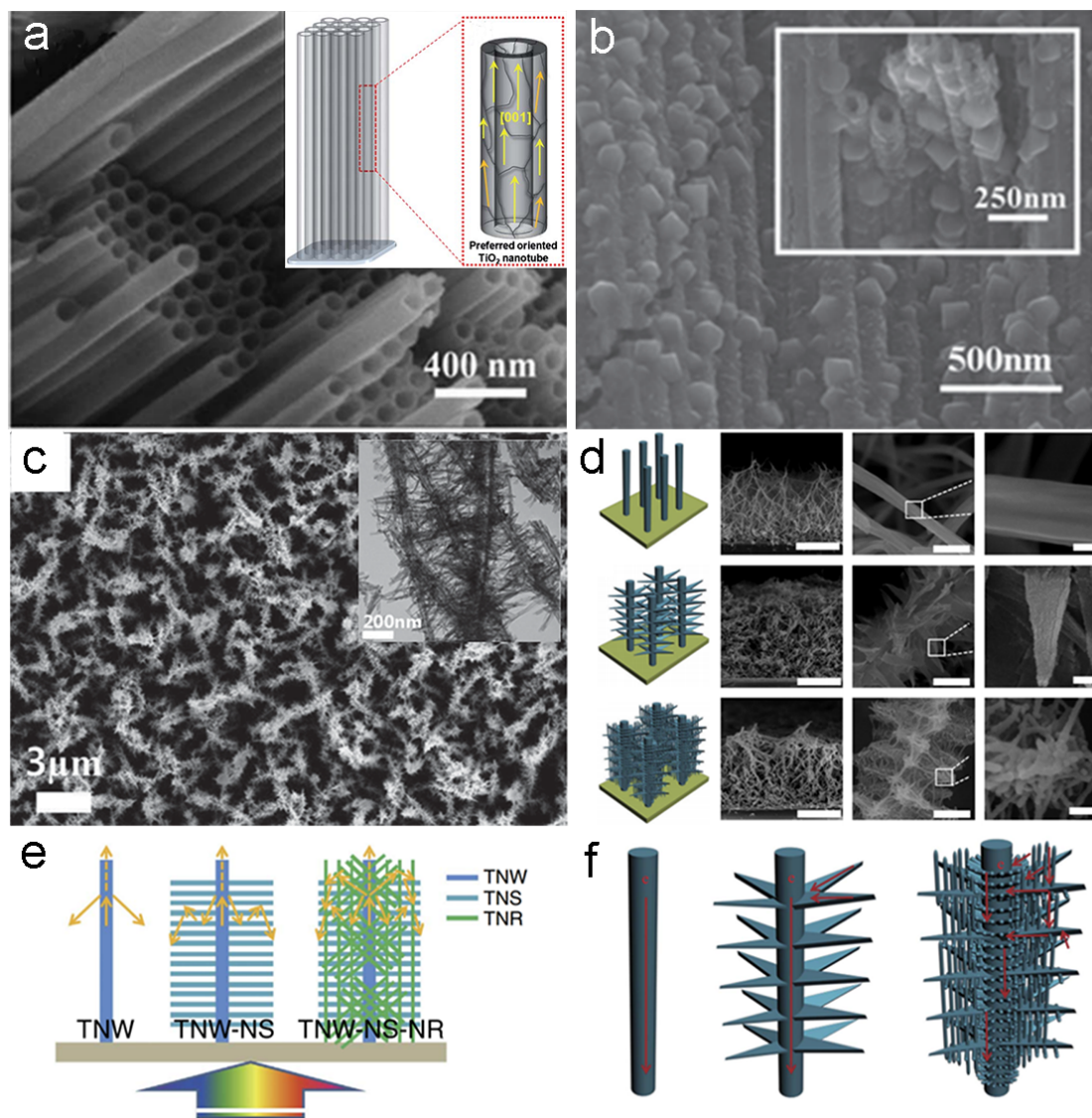


Figure 6. **a.** SEM image of the highly ordered TiO₂ nanotube array (reprinted with permission from ref. 37. Copyright 2012 Royal Society of Chemistry). **b.** Hierarchically structured TiO₂ nanotube arrays formed by subsequent hydrothermal processing (reprinted with permission from ref. 40. Copyright 2013 Wiley-VCH). **c.** SEM and TEM images of the hierarchical one-dimensional TiO₂ nanostructure (reprinted with permission from ref. 46. Copyright 2014 Wiley-VCH). **d.** Schematic structures and SEM images of TiO₂ hyperbranched arrays. **e, f.** Schematic illustration of light scattering and electron transport pathways within the simplified network of nanowire, branched nanowire and hyperbranched nanowire arrays (reprinted with permission from ref. 51. Copyright 2014 Nature Publishing Group).

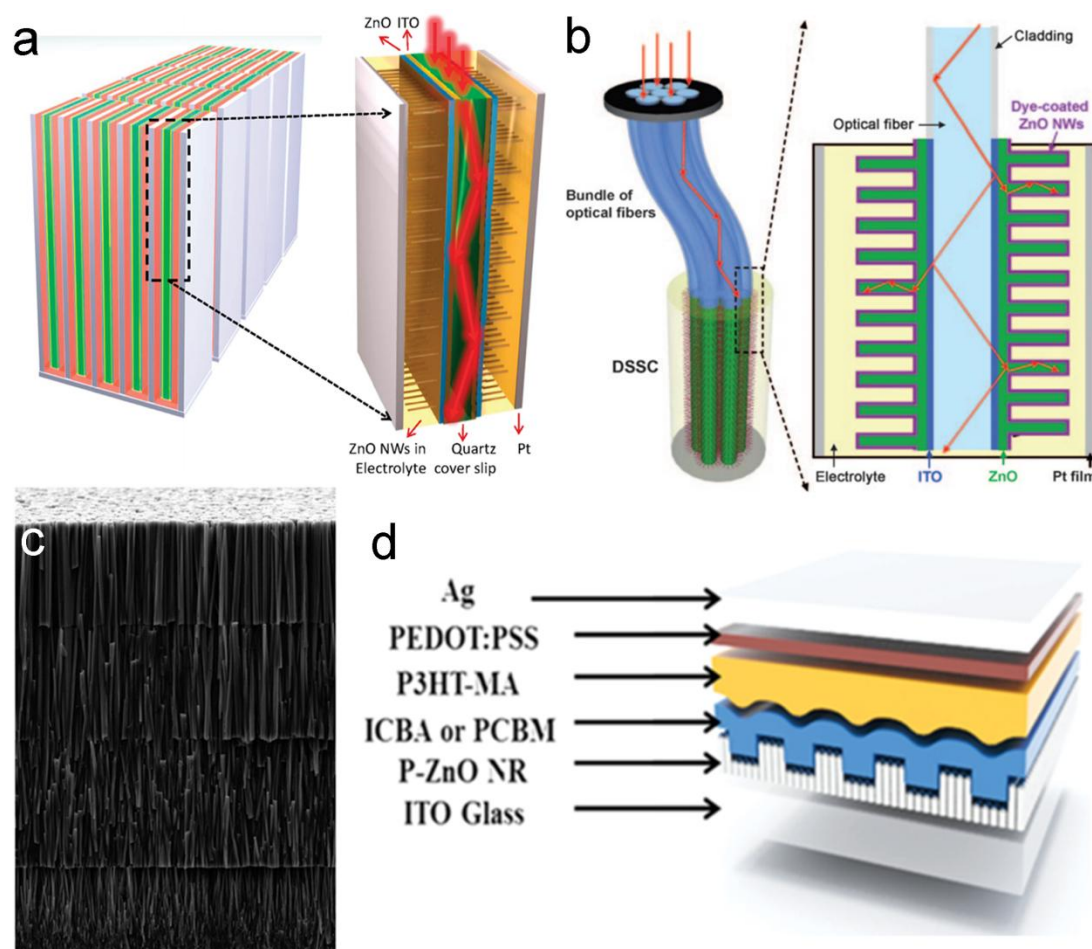


Figure 7. **a.** Schematic architecture of planar waveguide-nanowire integrated three-dimensional dye-sensitized solar cell (reprinted with permission from ref. 60. Copyright 2010 American Chemical Society). **b.** A three-dimensional dye-sensitized solar cell composed of optical fiber and ZnO nanowires grown vertically on the fiber surface (reprinted with permission from ref. 61. Copyright 2009 Wiley-VCH) **c.** SEM image of a four-layer assembly of ZnO nanowire arrays (reprinted with permission from ref. 62. Copyright 2011 American Chemical Society). **d.** A polymer solar cell based on P3HT/PC₆₀BM bilayer (reprinted with permission from ref. 71. Copyright 2014 Wiley-VCH).

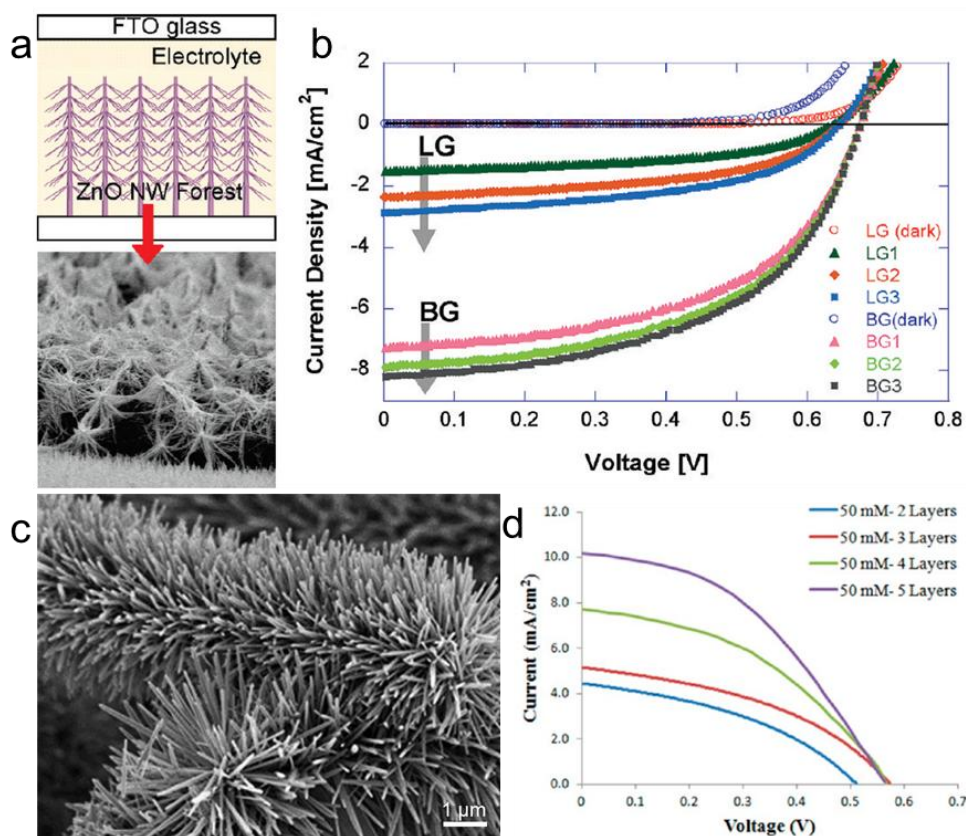


Figure 8. **a.** Schematic illustration and SEM image of ZnO nanowire forest. **b.** J-V curves of dye-sensitized solar cells based on the ZnO nanowire forest. (reprinted with permission from ref. 74 Copyright 2011 American Chemical Society). **c.** SEM image of highly dense caterpillar-like ZnO nanowire array. **d.** J-V curves for different layers of ZnO nanowire arrays (reprinted with permission from ref. 77. Copyright 2012 American Chemical Society).

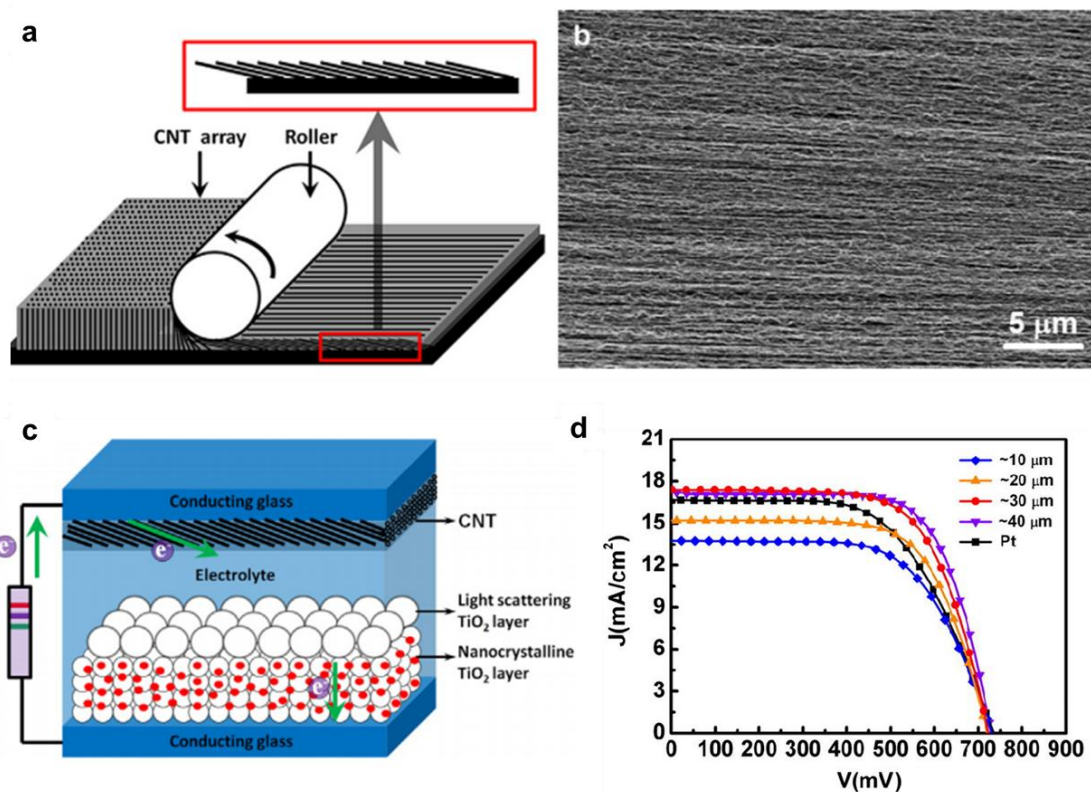


Figure 9. **a.** Schematic illustration to the preparation of penetrated and aligned CNT film. **b.** SEM image of the CNT film from a side view. **c.** Schematic illustration of the dye-sensitized solar cell with penetrated and aligned CNT film as counter electrode. **d.** J–V curves of dye-sensitized solar cells by using penetrated and aligned CNT films with different thicknesses and platinum film as counter electrodes under AM1.5 illumination (reprinted with permission from ref. 97. Copyright 2012 Elsevier B.V).

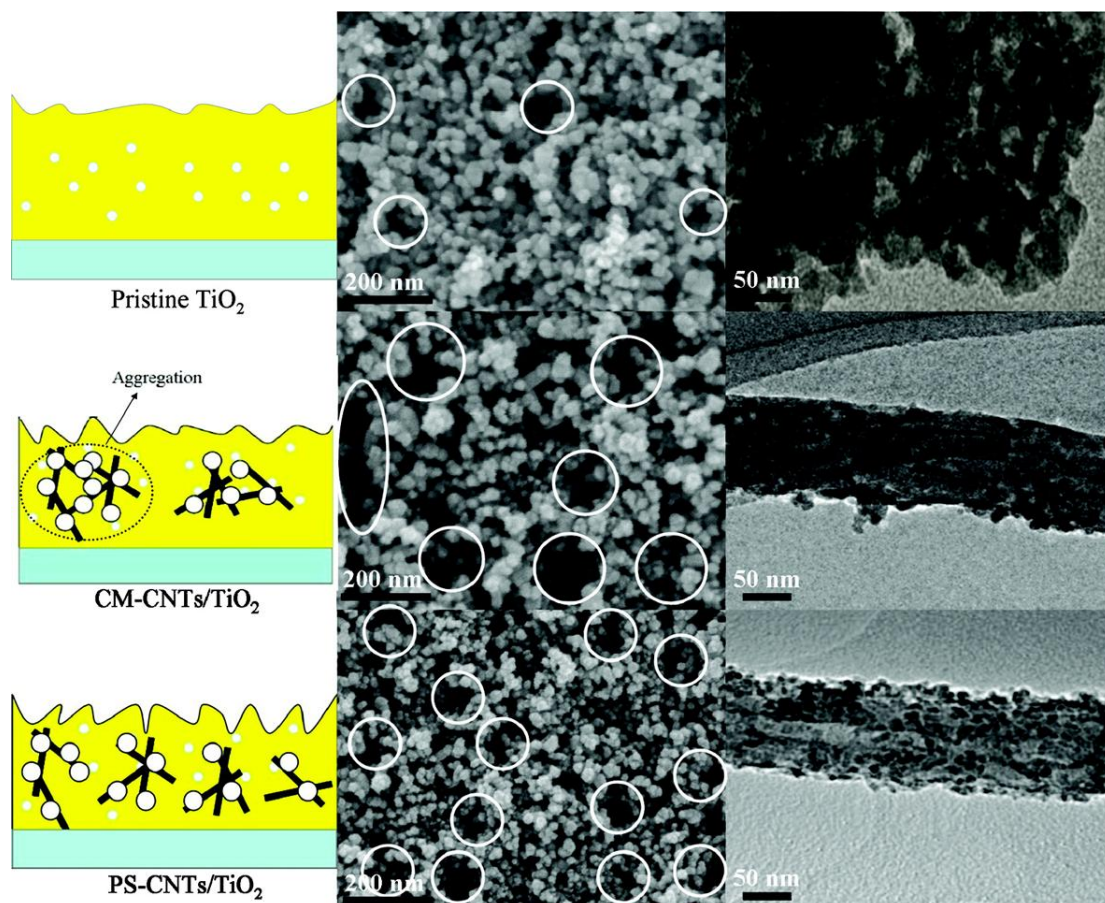


Figure 10. Schematic illustration (left), SEM (middle) and TEM images (right) of the pristine TiO₂, chemically modified-CNT/TiO₂ and plasma-treated CNT/TiO₂ hybrids (reprinted with permission from ref. 106. Copyright 2011 American Chemical Society).

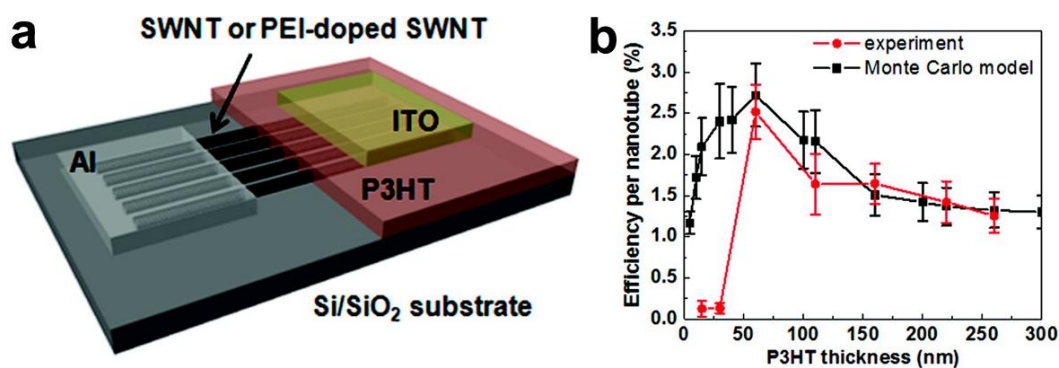


Figure 11. **a.** Schematic illustration to a planar heterojunction solar cell based on a P3HT film on laterally aligned single-walled CNTs. The device shares a width, length and height of 0.5 mm, 1 mm, and 15–260 nm, respectively, with the height depending on the thickness of P3HT. **b.** PCE per nanotube of the devices as a function of the P3HT thickness. The red circles are the experimental results from the devices with P3HT thicknesses ranging from 15 to 260 nm, and the black squares are the results calculated from the kinetic Monte Carlo model (reprinted with permission from ref. 111. Copyright 2010 American Chemical Society).

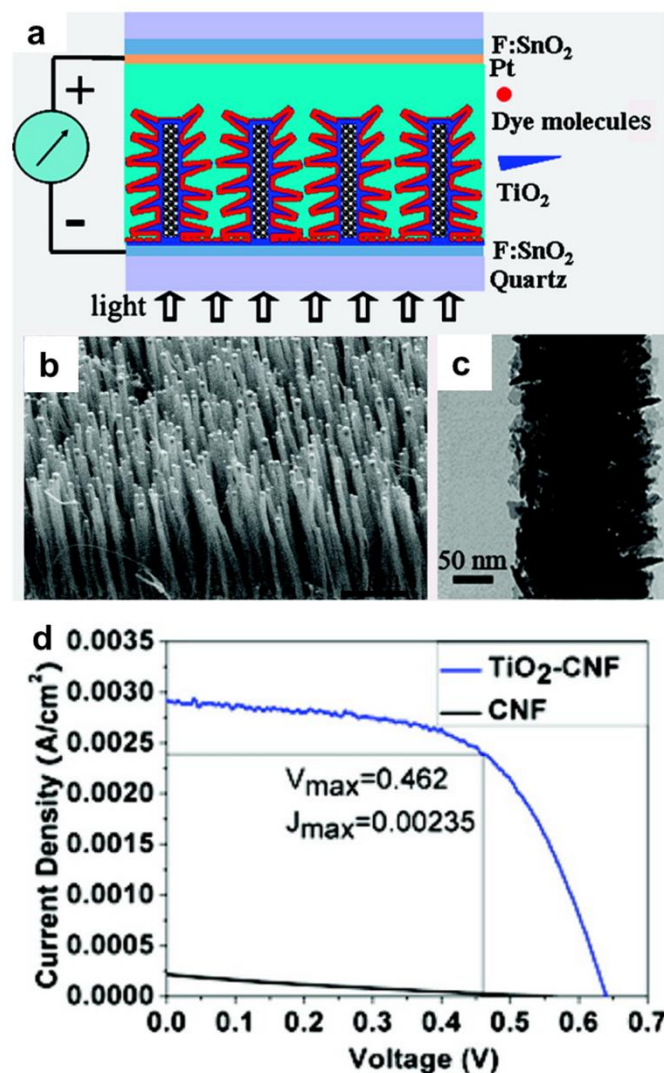


Figure 12. **a.** Schematic of vertically aligned carbon nanofiber arrays coated with anatase TiO₂ nano-needles for DSC. **b.** SEM image at a 45° perspective view of an as-fabricated vertically aligned carbon nanofiber array. **c.** TEM image of a carbon nanofiber after coating anatase TiO₂ nano-needles. **d.** J-V curves of dye-sensitized solar cells using as-fabricated vertically aligned carbon nanofibers (black line) and TiO₂-coated vertically aligned carbon nanofibers (blue line) as photoanodes (reprinted with permission from ref. 126. Copyright 2009 American Chemical Society).

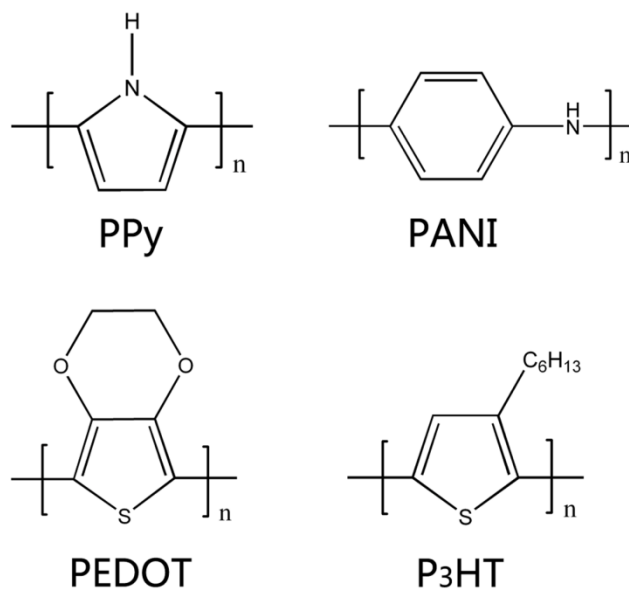


Figure 13. Molecular structures of representative conducting polymers.

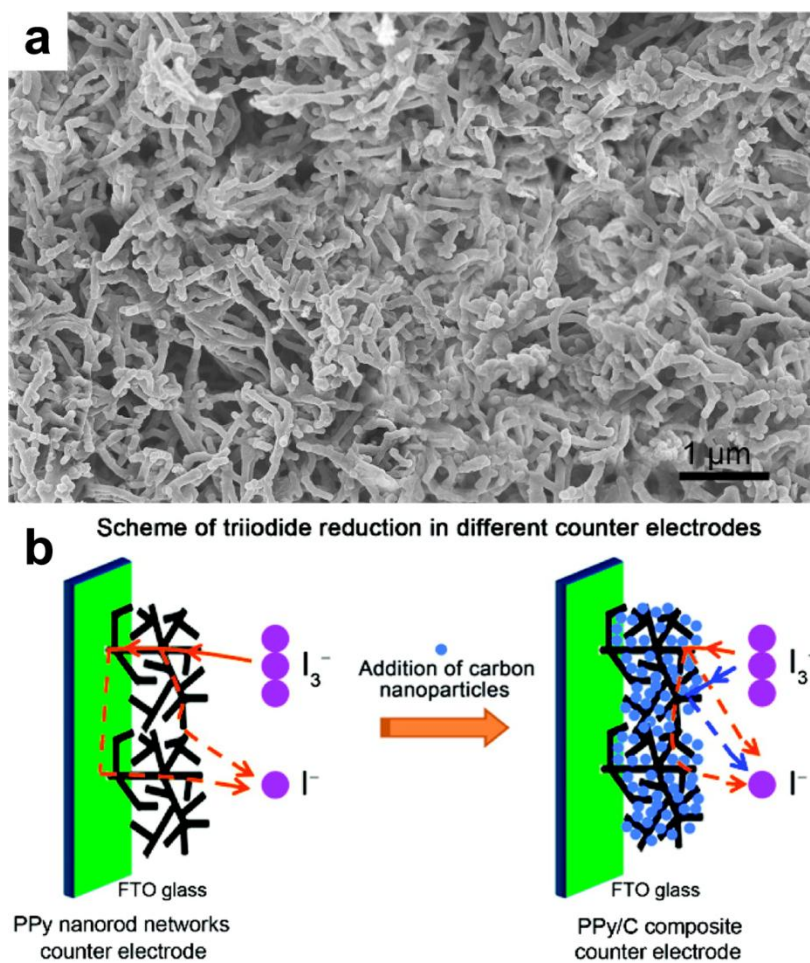


Figure 14. **a.** SEM image of PPy nanorods. **b.** Schematic illustration to the triiodide reduction on the PPy nanorod networks which served as the counter electrode in the dye-sensitized solar cell (reprinted with permission from ref. 136. Copyright 2011 American Chemical Society).

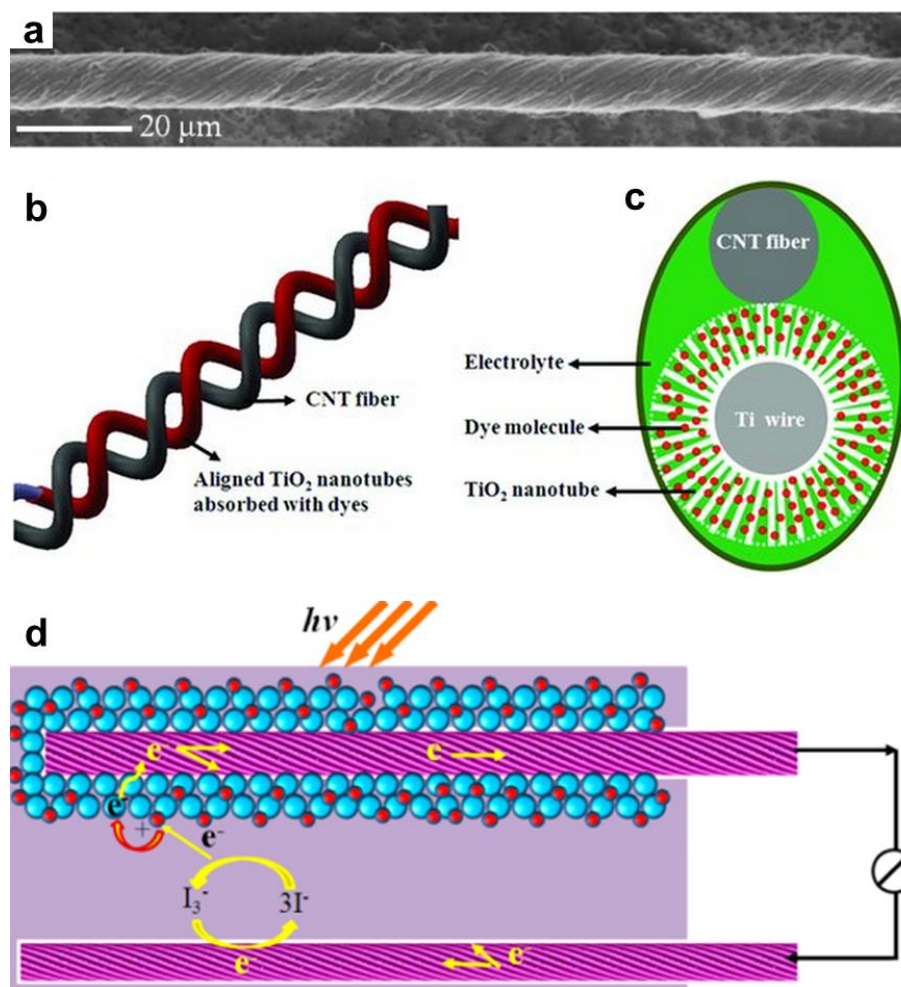


Figure 15. **a.** SEM image of a typical aligned CNT fiber. (reprinted with permission from ref. 154. Copyright 2012 American Chemical Society). **b, c.** Schematic illustration to the one-dimensional dye-sensitized solar cell using aligned CNT fiber as counter electrode by side and top views, respectively (reprinted with permission from ref. 155. Copyright 2012 Wiley-VCH). **d.** Schematic illustration to the one-dimensional dye-sensitized solar using aligned CNT fibers as both working and counter electrodes (reprinted with permission from ref. 154. Copyright 2012 American Chemical Society).

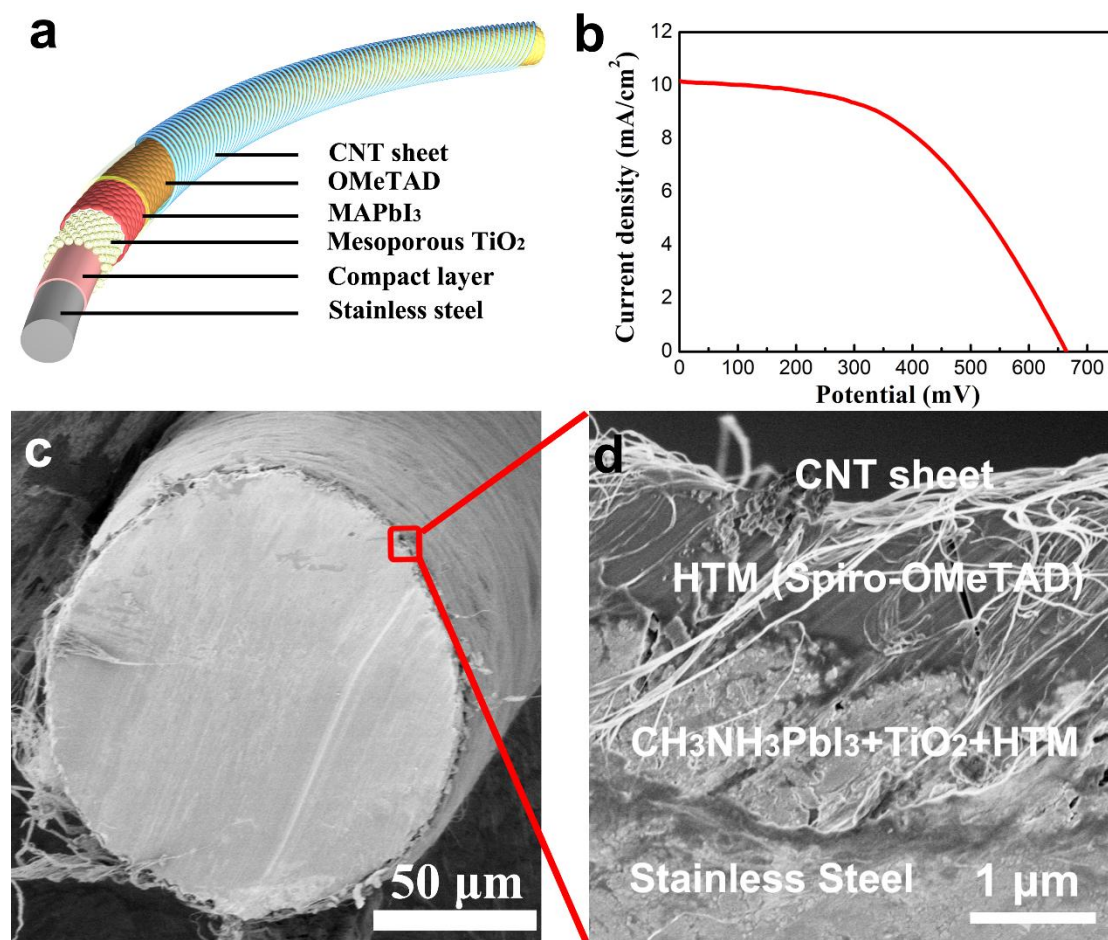


Figure 16. **a.** Structure illustration of one-dimensional perovskite solar cell. **b.** J-V curve of a typical perovskite solar cell with an efficiency of 3.3%. **c, d.** Cross-sectional SEM image of one-dimensional perovskite solar cell at low and high magnifications, respectively (reprinted with permission from ref. 164. Copyright 2014 Wiley-VCH).

Biographical Information



Hao Sun received his B. S. in Polymer Material and Engineering from Sun Yat-Sen University in 2012. He is currently a Ph.D. student majoring at Macromolecular Chemistry and Physics at Fudan University. His work focuses on the use of carbon nanomaterials in energy conversion and storage.



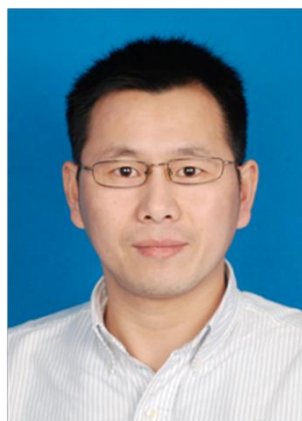
Jue Deng received his B. S. in Polymer Material and Engineering from Sun Yat-Sen University in 2013. He is currently a graduate student majoring at Macromolecular Chemistry and Physics at Fudan University. His work focuses on the use of carbon nanomaterials in multifunctional energy devices.



Longbin Qiu received his B.S. in Polymer Material and Engineering from Sun Yat-Sen University in 2011. He is currently a Ph.D. student majoring at Macromolecular Chemistry and Physics at Fudan University. His work focuses on the synthesis of carbon nanomaterials and their applications in dye-sensitized and perovskite solar cells.

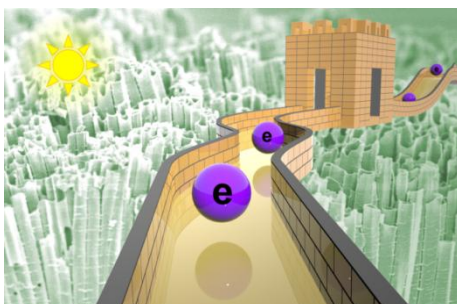


Xin Fang received his B.S. in Polymer Material and Engineering from Sichuan University in 2012. He is currently a graduate student majoring at Macromolecular Chemistry and Physics at Fudan University. His work focuses on the synthesis of carbon nanomaterials and their applications in energy conversion and storage.



Huisheng Peng is currently a professor at Department of Macromolecular Science and Laboratory of Advanced Materials at Fudan University. He received his B.E. in Polymer Materials at Donghua University in China in 1999, M.S. in Macromolecular Chemistry and Physics at Fudan University in China in 2003 and Ph.D. in Chemical Engineering at Tulane University in USA in 2006. He then worked at Los Alamos National Laboratory before joining Fudan University in 2008. He focuses on the development of miniature fiber-shaped solar cells, lithium ion batteries and supercapacitors and has published over 110 peer-reviewed papers.

Graphical abstract



Broader context: With the persistently growing demand for harvesting abundant and clean solar energy, increasing attentions are paid to develop efficient solar cells to remit the energy crisis in recent years. Material optimization is considered to be a key to improve the charge separation, transport and collection, resulting in better device performances. One-dimensional nanomaterials share the combined advantages of rapid charge transport and collection due to large specific surface areas and the one-dimensional configuration, and are widely used to build efficient solar cells. Herein, we systematically review the recent progress in efficient solar cells based on one-dimensional nanomaterials, selecting metal, metal oxide, carbon and conductive polymer as representatives. We also present the impact of one-dimensional configuration on device performance, and give a perspective on one-dimensional nanomaterials aiming at future solar cells.